Biochemical and Biophysical Research Communications 412 (2011) 296–301

Contents lists available at ScienceDirect

Biochemical and Biophysical Research Communications

journal homepage: www.elsevier.com/locate/ybbrc

Therapeutic potential of ghrelin treatment for unloading-induced muscle atrophy in mice

Keiichi Koshinaka, Koji Toshinai, Arif Mohammad, Kenji Noma, Miki Oshikawa, Hiroaki Ueno, Hideki Yamaguchi, Masamitsu Nakazato *

Division of Neurology, Respirology, Endocrinology and Metabolism, Department of Internal Medicine, Faculty of Medicine, University of Miyazaki, 5200 Kihara, Kiyotake, Miyazaki 889-1692, Japan

ARTICLE INFO

Article history:
Received 23 June 2011
Available online 28 July 2011

Keywords:
Ghrelin
Muscle atrophy
Mice
Growth hormone

ABSTRACT

Ghrelin is a growth hormone (GH) secretagogue secreted mainly from the stomach that functions in controlling muscle volume and energy homeostasis. We here studied the effects of ghrelin on unloading-induced muscle atrophy using a mouse model of hindlimb suspension (HS). Ghrelin administration during 2-week HS alleviated reductions of muscle mass in the fast-twitch fiber-rich plantaris muscle and the slow-twitch fiber-rich soleus muscle of the hindlimb. Ghrelin administration during a 5-day recovery period following 2-week HS enhanced food intake and facilitated recovery from atrophy in both muscles. Ghrelin administration normalized hypercorticosteronemia in these studies. Ghrelin's anti-muscle atrophy effect was found even under pair-feeding condition, but not in mice given des-acyl ghrelin. Insulin-like growth factor (IGF)-1 mRNA expression was significantly reduced in the atrophied plantaris muscle compared with control muscles. A single ghrelin administration to HS mice acutely increased plasma GH and also amplified phosphorylation of signal transducer and activator of transcription (STAT) 5 and increased IGF-1 mRNA expression in the plantaris muscle, but not in the soleus muscle. This study demonstrated that ghrelin stimulated the GH-STAT5-IGF-1 axis in the locally atrophied plantaris muscle, and its administration alleviated muscle atrophy and facilitated recovery from muscle atrophy. Ghrelin's effects represent a novel therapeutic paradigm for the treatment of unloading-induced muscle atrophy induced by factors such as bed rest, injury, and joint immobilization.

1. Introduction

Mechanical stress on skeletal muscles is one of the critical factors controlling muscle mass. The maintenance of muscle mass is regulated by a balance between protein synthesis and breakdown. Muscle atrophy is a common phenomenon observed in a wide variety of unloading-related situations, including bed rest, injury, joint immobilization, and reduced physical activity associated with aging [1]. A number of different agents from diverse chemical classes have entered clinical trials for the treatment of muscle atrophy, but none have yet been approved for clinical use.

Ghrelin is a 28-amino acid peptide initially isolated from human and rat stomachs as an endogenous ligand of the growth hormone (GH) secretagogue (GHS) receptor (GHS-R) [2]. Ghrelin is predominantly produced by a distinct type of endocrine cell of the gastric oxyntic glands [3] and acts on the pituitary to stimulate GH release and on the hypothalamus to enhance food intake [2,4]. Ghrelin peptides exist in two major molecular forms, *n*-octanoylated ghrelin and des-*n*-octanoyl ghrelin (des-acyl ghrelin) [2]. Acylation at the third amino acid residue is necessary for the binding of ghrelin to the GHS-R; thus, the acylated form was designated as ghrelin in the original description [2].

GH plays a key role in controlling postnatal somatic growth of multiple tissues, including skeletal muscle, and its anabolic effect is mediated by insulin-like growth factor 1 (IGF-1) [5]. Chronic ghrelin administration increased circulating levels of IGF-1 [6] and promoted adiposity and body weight gain in rodents [7,8]. Ghrelin administration also exerted an anti-muscle atrophy effect in malnutrition-associated whole-body catabolic conditions observed in cachectic patients [9] and rodents [6,10,11], as well as in rodents undergoing long-term fasting [12]. However, ghrelin's therapeutic potential for the treatment of unloading-induced muscle atrophy whose primary cause is loss of mechanical stress to muscles rather than malnutrition has not been investigated.

Unloading-induced muscle atrophy was found in restricted and unloaded muscles in which there was reduced local IGF-1 production [13]. Also, up-regulated expression of the atrogin-1 gene, a muscle-specific ubiquitin ligase, in the atrophied muscles [14] suggested that the ubiquitin–proteasome pathway responsible for the molecular pathogenesis of muscle wasting was activated. Continuous ghrelin administration to healthy subjects activated muscle

* Corresponding author. Fax: +81 985 85 1869.
E-mail address: nakazato@med.miyazaki-u.ac.jp (M. Nakazato).

0006-291X/$ - see front matter © 2011 Elsevier Inc. All rights reserved.
doi:10.1016/j.bbrc.2011.07.086

signal transducer and activator of transcription (STAT) 5, a transcription factor that mediates IGF-1 gene transcription [15]. GH also has the potential to activate muscle insulin signaling [16,17]. Insulin signaling activation was found to down-regulate atrogin-1 gene expression [18] and prevent unloading-induced muscle atrophy [19]. Although no study has examined the effect of ghrelin administration on muscle GH or insulin signaling in atrophied muscles induced by unloading, these activations of STAT5 and insulin signaling might bring about the anti-muscle atrophy effect of ghrelin.

The present study aimed to investigate the efficacy of ghrelin at preventing and alleviating unloading-induced muscle atrophy. Hindlimb suspension (HS) is an animal model of unloading-induced muscle atrophy [13,19]. We conducted both a preventive and therapeutic study using a mouse model of HS-induced muscle atrophy. In the former, we administered ghrelin daily during a 2-week HS period. In the latter, we administered ghrelin daily for 5 days after HS-induced muscle atrophy had developed. Skeletal muscle fibers are classically divided into either type I (slow-twitch) or type II (fast-twitch) fibers. We examined two different types of muscles in the hindlimb, the plantaris muscle (rich in fast-twitch fibers) and the soleus muscle (rich in slow-twitch fibers).

2. Materials and methods

2.1. Treatment of animals

We used 7-week-old male C57BL/6 mice (Charles River Japan, Inc., Numazu, Japan). Animals were housed individually at constant room temperature (23 ± 1 °C) in a 12-h light (08:00–20:00 h)/12-h dark cycle and were provided standard laboratory chow and water *ad libitum*. All mice were kept fasting for 3 h before blood and muscle samplings. The experimental protocol was approved by the Ethics Review Committee for Animal Experimentation of the Faculty of Medicine, University of Miyazaki.

2.2. Experiment I: effects of chronic ghrelin administration on muscle atrophy

Mice underwent HS for 2 weeks as reported previously [13,19]. During this period, they were given twice-daily (09:00 and 17:00) subcutaneous injections of 100 μl saline or ghrelin (107 nmol/kg BW, Asbio Pharma, Kobe, Japan) dissolved in 100 μl saline. The first injection was performed at 17:00 on day 0 and the last injection at 17:00 on day 13. Mice in the sedentary group were kept in normal housing for 2 weeks and given saline injections on the same schedule as the HS group. On day 14 (09:00), all were anesthetized by intraperitoneal injection of sodium pentobarbital (50 mg/kg BW). Blood was taken by heart puncture. Plantaris and soleus muscles and epididymal fat were dissected out and weighed. For the corticosterone measurement, blood was taken from the other mice by decapitation.

2.3. Experiment II: effects of chronic ghrelin administration on recovery from muscle atrophy

After the 2-week HS, mice were kept in normal housing for 5 days. During this recovery period, mice were given twice-daily subcutaneous injections of saline or ghrelin as described in Experiment I, and were maintained under *ad libitum* feeding or pair-feeding condition controlled by daily food intake measurement. The first injection was performed at 17:00 on day 0 and the last injection was at 17:00 on day 4. On day 5 (09:00), mice were sacrificed under anesthesia with sodium pentobarbital. Blood and tissue samplings were performed as described in Experiment I. For the corticosterone measurement, blood was taken from the other mice by decapitation on day 2. As a parallel experiment, mice were injected with des-acyl ghrelin instead of ghrelin at a dose of 107 nmol/kg body weight under *ad libitum* feeding condition.

2.4. Experiment III: single-dose ghrelin administration to HS mice: effects on blood parameters and atrophied muscles

Mice underwent HS for 2 weeks. On the last day of this 2-week period, ghrelin (107 nmol/kg BW) was subcutaneously injected while mice were kept in an HS posture, and blood was taken by decapitation 10 or 120 min after ghrelin injection. As a parallel experiment, mice were sacrificed 10 or 120 min after ghrelin injection under sodium pentobarbital anesthesia, and the plantaris and soleus muscles were removed and immediately clamp-frozen in liquid nitrogen for Western blot analysis and real-time quantitative PCR.

2.5. Western blot analysis

Plantaris and soleus muscles were homogenized in ice-cold buffer containing 50 mM HEPES (pH 7.6), 150 mM NaCl, 10% glycerol, 1% IGEPAL, 1 mM $MgCl_2$, 2 mM EDTA, 20 mM $Na_4P_2O_7$, 20 mM glycerophosphate, 10 mM NaF, 2 mM Na_3VO_4, 2 mM PMSF, 1 mM $CaCl_2$, aprotinin (10 μg/mL) and leupeptin (10 μg/mL) [20]. The homogenates were then rotated end-over-end at 4 °C for 60 min, and centrifuged at 10,000*g* for 10 min at 4 °C. Aliquots of the supernatants were used for Western blot analysis. Samples on PVDF membranes were incubated overnight with antibodies against p-STAT5 Tyr^{694} (1:2000; Cell Signaling Technology, Beverly, MA) and p-Akt Thr^{308} (1:2000; Cell Signaling Technology) at 4 °C, followed by incubation for 90 min with HRP-conjugated anti-rabbit IgG (1:4000; Cell Signaling Technology). Immunoreactive bands were visualized by enhanced chemiluminescence reagent (GE Healthcare Japan, Hino, Japan) and quantified using NIH images.

2.6. RNA extraction and real-time quantitative PCR

Total RNA was isolated from plantaris and soleus muscles using RNA extraction reagent (RNA-Bee: TEL-TEST, Friendswood, TX). After DNase I treatment (Invitrogen, Carlsbad, CA), the total RNA was reverse-transcribed using the Superscript III system (Invitrogen). To quantify the relative expression levels of IGF-1 and atrogin-1 mRNA, quantitative real-time PCR was carried out with SYBR premix Ex Taq (Takara Bio, Otsu, Japan). The obtained values were normalized with the value for glyceraldehydephosphate dehydrogenase (GAPDH) as an internal control gene. The primers were as follows: 5′-CTGAGCTGGTGGATGCTCTT-3′ (sense) and 5′-CACTCATCC ACAATGCCTGT-3′ (antisense) for IGF-1, 5′-TGGGTGTATCGGATGGA-GAC-3′ (sense) and 5′-TCAGCCTCTGCATGATGTTC-3′ (antisense) for atrogin-1, 5′-TCAAGAAGGTGGTGAAGCAG-3′ (sense) and 5′-TGGG AGTTGCTGTTGAAGTC-3′ (antisense) for GAPDH.

2.7. Blood parameters

Blood glucose was measured using the Medisafe-Mini system (Terumo, Tokyo, Japan). Plasma GH (SPI-BIO, Montigny le Bretonneux, France), insulin (Morinaga Institute of Biological Science, Yokohama, Japan), IGF-1 (R&D Systems, Minneapolis, MN), and corticosterone (AssayPro, St. Charles, MO) were determined using EIA kits according to the manufacturer's instructions.

2.8. Statistics

Data are expressed as means ± SE. Differences among multiple groups were determined using a one-way analysis of variance

and subsequently Fisher's least significant difference method. When two mean values were compared, analysis was performed by unpaired *t*-test. $P < 0.05$ was considered significant.

3. Results

3.1. Experiment I: chronic ghrelin administration alleviated HS-induced atrophy of plantaris muscles

The upper panel in Table 1 shows mouse characteristics and blood parameters at the end of 2-week HS. Body weight and epididymal fat weight of HS mice were significantly lower than those of sedentary mice. The weights of plantaris and soleus muscles of HS mice were 21% and 46% lower than those of sedentary mice, respectively. Ghrelin administration did not affect body weight or epididymal fat weight in HS mice; however, it significantly raised the weight of the plantaris muscle, but not the soleus muscle, compared to HS/saline mice. There were no significant differences among the three groups in terms of blood glucose levels or concentrations of plasma insulin, GH, or IGF-1. HS significantly elevated plasma corticosterone concentrations; however, this elevation was completely abolished by ghrelin administration.

3.2. Experiment II: chronic ghrelin treatment facilitated recovery from HS-induced muscle atrophy

After the discontinuation of 2-week HS, mice were kept in normal housing with or without 5-day ghrelin administration. The lower panel in Table 1 shows mouse characteristics and blood parameters at the end of the 5-day recovery period. The mean body weight of the ghrelin group was significantly greater than that of the saline group. There was a tendency toward increased fat weight in the ghrelin group compared with the saline group, but this difference was not significant ($P = 0.06$). Plantaris and soleus muscle weights in the ghrelin group were significantly greater than those in the saline group. In the ghrelin group, blood glucose levels, but not concentrations of plasma insulin, GH, or IGF-1, were significantly lower than those in the saline group. HS-induced hypercorticosteronemia was still found even 2 days after the cessation of HS in the saline group, but was attenuated by ghrelin administration.

Table 1
Effects of ghrelin administration on mouse characteristics and blood parameters.

	Sedentary saline	HS saline	HS ghrelin
Experiment I (ghrelin administration during 2-week HS period)			
Body weight (g)	24.0 ± 0.5	22.1 ± 0.2*	22.6 ± 0.4*
Epididymal fat weight (mg)	292 ± 21	180 ± 13*	222 ± 24*
Plantaris muscle weight (mg)	15.4 ± 0.5	12.2 ± 0.4*	13.7 ± 0.2*#
Soleus muscle weight (mg)	8.9 ± 0.8	4.8 ± 0.2*	5.2 ± 0.1*
Blood glucose (mg/dL)	108 ± 6	124 ± 9	106 ± 5
Insulin (ng/mL)	1.5 ± 0.1	1.8 ± 0.2	1.9 ± 0.1
GH (ng/mL)	13.6 ± 1.2	12.0 ± 1.4	13.9 ± 2.0
IGF-1 (ng/mL)	312 ± 11	303 ± 13	307 ± 13
Corticosterone (ng/mL)	71 ± 8	221 ± 45*	109 ± 25#
Experiment II (ghrelin administration during 5-day recovery period)			
Body weight (g)		23.2 ± 0.2	24.2 ± 0.4#
Epididymal fat weight (mg)		216 ± 17	264 ± 16
Plantaris muscle weight (mg)		14.8 ± 0.2	15.9 ± 0.4#
Soleus muscle weight (mg)		7.0 ± 0.2	7.9 ± 0.3#
Blood glucose (mg/dL)		148 ± 7	117 ± 6#
Insulin (ng/mL)		1.5 ± 0.2	2.0 ± 0.2
GH (ng/mL)		9.7 ± 1.6	15.5 ± 3.9
IGF-1 (ng/mL)		325 ± 5	309 ± 6
Corticosterone (ng/mL)		237 ± 43	126 ± 20#

Values are means ± SE ($n = 5$–9). HS: hindlimb suspension.
* $P < 0.05$ vs. sedentary group.
\# $P < 0.05$ vs. HS/saline group.

3.3. Experiment II: ghrelin administration facilitated recovery from plantaris muscle atrophy

Five-day ghrelin administration to mice fed *ad libitum* significantly enhanced food intake compared with other groups (Fig. 1A). Body weights of all four groups of HS mice were significantly lower than that of the sedentary group at day 0 (the end of the HS period) (Fig. 1B). Body weights of ghrelin-treated mice fed *ad libitum* gradually increased throughout the recovery period, reaching comparable levels as the sedentary group at day 3 (though the similarity was not statistically significant), then at day 4 achieving statistical significance compared with the HS/saline group. Body weights of HS/pair-fed and HS/des-acyl ghrelin groups were similar to that of the HS/saline group throughout the 5 days. Ghrelin administration recovered plantaris muscle weights of both *ad libitum* and pair-fed groups (Fig. 1C). Ghrelin administration to HS mice fed *ad libitum* completely recovered their soleus muscle weights; however, soleus muscle recovery was not observed in the pair-fed group (Fig. 1D). Des-acyl ghrelin did not facilitate the recovery of either the plantaris or soleus muscles (Fig. 1C and D).

3.4. Experiment III: ghrelin stimulated GH signaling in atrophied muscles

The plasma GH concentration in HS mice increased 20-fold above the basal level 10 min after a single subcutaneous ghrelin administration (Fig. 2A), and returned to the basal level at 120 min. Plasma insulin was lower than the basal level 10 min after ghrelin administration, but the decline was not statistically significant ($P = 0.06$; Fig. 2B). Ghrelin administration did not alter the concentrations of plasma IGF-1 (Fig. 2C) or corticosterone (Fig. 2D). Two-week HS did not affect basal STAT5 phosphorylation in either plantaris or soleus muscles (Fig. 3A). Ghrelin increased STAT5 phosphorylation in both muscles 10 min after administration. HS significantly decreased Akt phosphorylation in the soleus muscle, but not the plantaris muscle (Fig. 3A). Ghrelin administration did not increase Akt phosphorylation. In both muscles, IGF-1 mRNA amounts in the HS/saline group were significantly lower than those in the respective muscles in sedentary mice (Fig. 3B). Ghrelin enhanced IGF-1 mRNA expression in the plantaris muscle, but not the soleus muscle, 120 min after the injection (Fig. 3B). HS enhanced mRNA expression of atrogin-1 in the soleus muscle (Fig. 3B). Ghrelin did not change atrogin-1 mRNA expression in either muscle (Fig. 3B).

4. Discussion

Several studies have shown that chronic ghrelin or GHS-R agonist administration results in the preservation of muscle mass or lean body mass with increased food intake as well as body weight gain in whole-body catabolic conditions associated with malnutrition [7,10–12]. In the present study, we demonstrated for the first time that ghrelin administration was effective at alleviating muscle mass loss and facilitating recovery from unloading-induced muscle atrophy, the primary cause of which is loss of mechanical stress on muscles.

The ghrelin dose used in this study, 107 nmol/kg BW, stimulated food intake and body weight gain. In unloading-induced muscle atrophy, ghrelin-induced body weight gain would be a positive factor due to its anti-muscle atrophy effect when atrophied muscles are being used, as was the case in Experiment II. This hypothesis was supported by the finding that ghrelin's anti-muscle atrophy effect in the soleus muscle, a typical anti-gravity muscle, was observed in Experiment II, but not in Experiment I. In contrast,

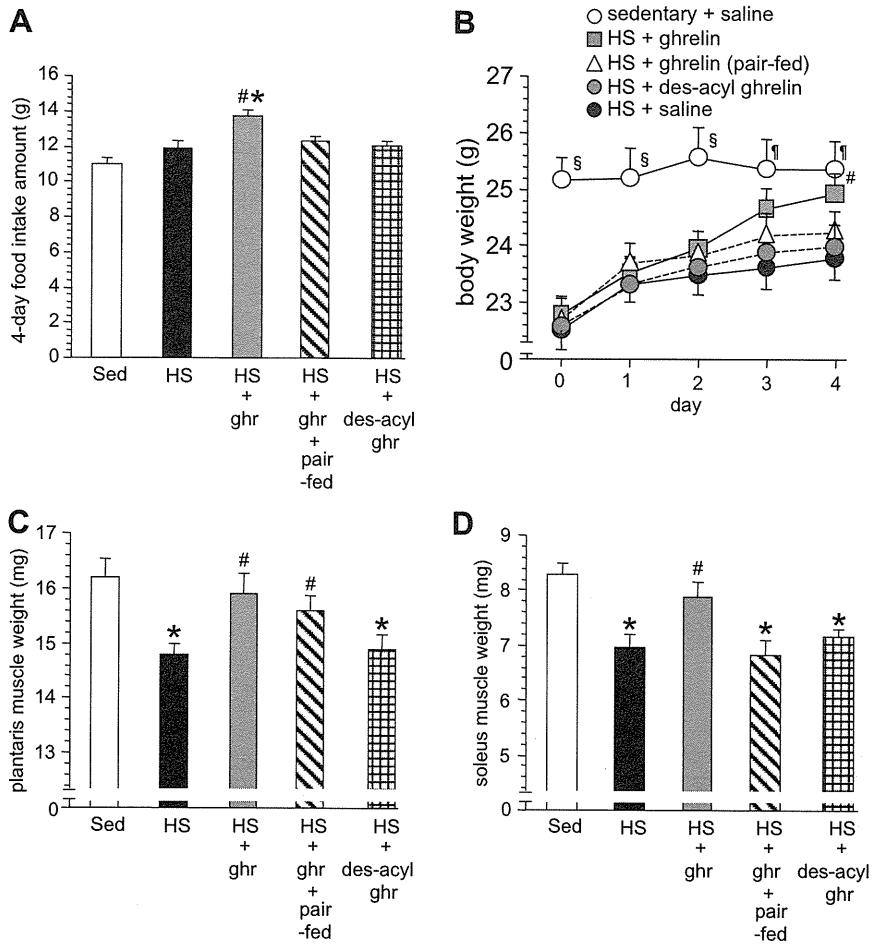

Fig. 1. Effects of 5-day ghrelin administration following 2-week HS on food intake and muscle weights (Experiment II). Ghrelin significantly increased food intake (A) and body weight (B) compared with four comparison groups. Ghrelin administration completely recovered muscle weights in the plantaris (C) and soleus (D) muscles. Ghrelin's anti-atrophy effect was observed in the plantaris muscle but not in the soleus muscle in pair-fed mice. Des-acyl ghrelin administration was ineffective in both muscles. Mice were fed *ad libitum* unless indicated as pair-fed. Values are expressed as means ± SE (n = 6–9). $^{*}P < 0.05$ vs. sedentary group, $^{\#}P < 0.05$ vs. HS group. $^{\S}P < 0.05$ vs. other groups. $^{*}P < 0.05$ vs. other groups except ghrelin group. Sed: sedentary, HS: hindlimb suspension, ghr: ghrelin.

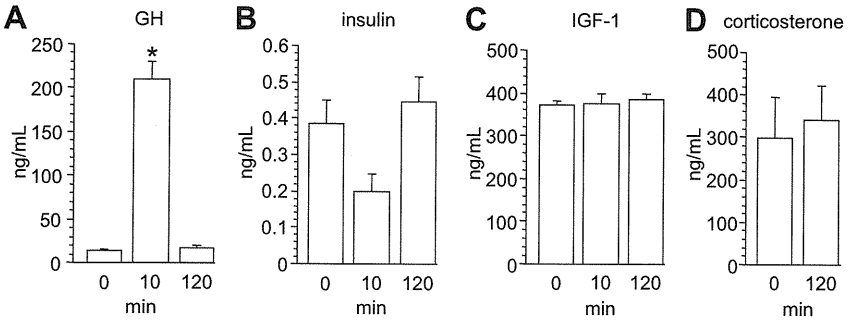

Fig. 2. Effects of single-dose ghrelin administration to HS mice on blood parameters (Experiment III). On the last day of a 2-week HS period, a single subcutaneous injection of ghrelin to HS mice being maintained in the HS posture increased plasma GH (A), but not insulin (B), IGF-1 (C), or corticosterone (D). Values are expressed as means ± SE (n = 4–9). $^{*}P < 0.05$ vs. values at 0 min.

the anti-muscle atrophy effect was observed in the plantaris muscle in both Experiments I and II. Given that ghrelin administration was also effective on the plantaris muscle of pair-fed mice without significant body weight gain, factors other than ghrelin's promotion of food intake could be responsible for its anti-muscle atrophy effect, at least in the plantaris muscle.

We showed that ghrelin's orexigenic effect was independent of its stimulation of GH secretion [4]. Ghrelin's stimulatory effect on GH secretion in HS mice might be a critical factor for the anti-muscle atrophy effect. The major portion of circulating IGF-1 is synthesized by the liver in response to GH [5]. Circulating IGF-1 was shown to be decreased under whole-body catabolic conditions such as cachectic adjuvant-induced arthritis, while 8-day administration of GH-releasing peptide-2 (GHRP-2), a GHS-R agonist, resulted in an increase in plasma IGF-1 level and prevention of muscle atrophy [21]. In the present study, HS did not reduce circulating IGF-1 levels,

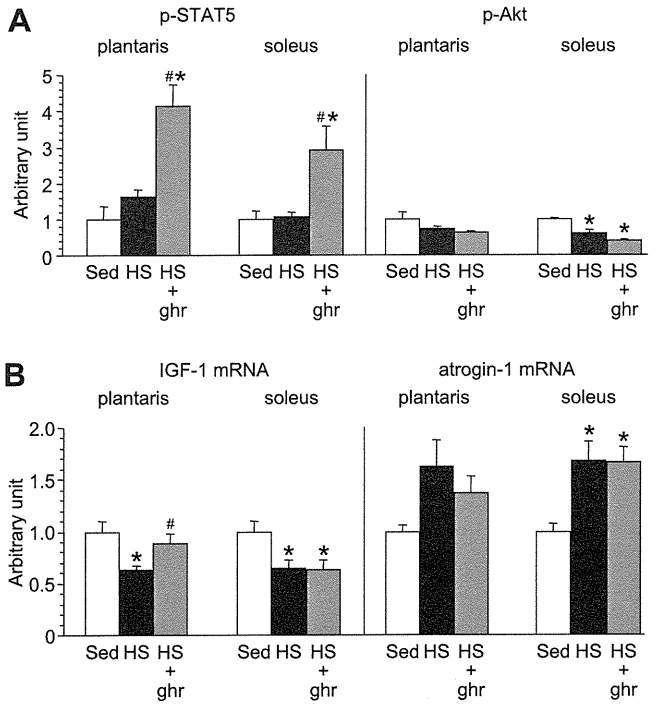

Fig. 3. Effects of single-dose ghrelin administration to HS mice on protein phosphorylation and gene expression in atrophied muscles (Experiment III). On the last day of a 2-week HS period, a single subcutaneous injection of ghrelin to HS mice being maintained in the HS posture increased STAT5 phosphorylation, but not Akt phosphorylation, in both plantaris and soleus muscles 10 min after the administration (A). Ghrelin also enhanced IGF-1 mRNA expression in plantaris muscles, but not soleus muscles, 120 min after the administration (B). Ghrelin did not change atrogin-1 mRNA expression in either muscle (B). Values are expressed as means ± SE ($n = 4–9$). $^{*}P < 0.05$ vs. sedentary group, $^{\#}P < 0.05$ vs. HS group. Sed: sedentary, HS: hindlimb suspension, ghr: ghrelin.

and neither single nor chronic ghrelin administrations increased them. Although we cannot explain the different IGF-1 responses between these two studies, our findings suggested that circulating IGF-1 was unlikely to have participated in the anti-muscle atrophy effect in this local atrophy model. In the present study, IGF-1 mRNA expression in both plantaris and soleus muscles were reduced by HS. We demonstrated here for the first time that ghrelin stimulated the GH-STAT5-IGF-1 axis in atrophied plantaris muscles. This may be a plausible explanation for the mechanism underlying the anti-muscle atrophy effect of ghrelin in the plantaris muscle. The finding that administration of des-acyl ghrelin, which lacks GH secretion activity, failed to induce the anti-muscle atrophy effect provides further support for our interpretation. In atrophied soleus muscles, ghrelin amplified STAT5 phosphorylation, but did not increase IGF-1 mRNA. Because we used only one sampling point for the analysis of mRNA, we could not exclude the possibility that ghrelin amplified IGF-1 mRNA in the soleus muscle. However, taken together with the differences between the two muscles in terms of anti-muscle atrophy effects and IGF-1 mRNA responses, it would appear that muscle characteristics, i.e., muscle fiber types, should be taken into account in evaluating the potency of ghrelin's anti-muscle atrophy effect.

GH administration to rats [16] and humans [17] has been shown to activate muscle insulin-signaling molecules, including Akt. Thirone et al. [16] reported that the intravenous administration of GH (1.8 mg/kg BW) activated insulin signaling in muscles, as judged by increased tyrosine phosphorylation of insulin receptor substrate-1, an upstream molecule of Akt. However, we did not find Akt activation in atrophied muscles after ghrelin administration despite a significant increase in GH level. In our preliminary experiments, when two mice were administered GH at a dose of 1.8 mg/kg BW, plasma GH rose up to 31,069 ± 2510 ng/mL (unpublished observation), which was markedly different from the level observed after ghrelin administration (200–300 ng/mL). Given this finding, we considered it unlikely that ghrelin activated muscle insulin signaling via GH-induced mechanisms.

Overexpression of early inflammatory cytokine genes such as TNF-α, IL-1, and IL-6, as well as related hypercorticosteronemia, are responsible for the molecular pathogenesis of muscle wasting [22–24]. Interestingly, continuous 24-h ghrelin administration to rats with thermal injuries [22] or 8-day GHRP-2 administration to experimental arthritis-induced cachectic rats [21,24] normalized the hypercorticosteronemia and the overexpression of these cytokine genes in atrophied muscles. The hypercorticosteronemia in HS mice was completely normalized by chronic ghrelin administration, suggesting that the anti-inflammatory effect of ghrelin might also contribute to the anti-muscle atrophy effect in the present study.

At clinical levels, the findings of Nagaya et al. [9] that chronic ghrelin administration to cachectic patients with chronic heart failure increased food intake, lean body mass, and muscle strength, suggest that ghrelin exerts a powerful anti-muscle atrophy effect in humans. However, it is not clear whether ghrelin might be effective in locally atrophied muscles induced by unloading in non-cachectic humans. Our present study using a mouse model of HS mice demonstrated that (1) ghrelin administration acutely stimulated the GH-STAT5-IGF1 axis in locally atrophied muscles, (2) chronic ghrelin administration alleviated muscle atrophy during HS and facilitated recovery afterward, and (3) ghrelin's anti-muscle atrophy effect was partially independent of the promotion of food intake. We conclude that ghrelin administration has therapeutic potential for the treatment of local muscle atrophy related to unloading, for instance due to bed rest, injury, joint immobilization, or aging.

Acknowledgments

This work was supported by MEXT KAKENHI 22126009, The Takeda Science Foundation, The Foundation for Growth Science. K. Koshinaka was supported by the Japan Foundation for Aging and Health.

References

[1] R.T. Jagoe, A.L. Goldberg, What do we really know about the ubiquitin-proteasome pathway in muscle atrophy?, Curr Opin. Clin. Nutr. Metab. Care 4 (2001) 183–190.
[2] M. Kojima, H. Hosoda, Y. Date, M. Nakazato, H. Matsuo, K. Kangawa, Ghrelin is a growth-hormone-releasing acylated peptide from stomach, Nature 402 (1999) 656–660.
[3] Y. Date, K. Toshinai, S. Koda, M. Miyazato, T. Shimbara, T. Tsuruta, A. Niijima, K. Kangawa, M. Nakazato, Peripheral interaction of ghrelin with cholecystokinin on feeding regulation, Endocrinology 146 (2005) 3518–3525.
[4] M. Nakazato, N. Murakami, Y. Date, M. Kojima, H. Matsuo, K. Kangawa, S. Matsukura, A role for ghrelin in the central regulation of feeding, Nature 409 (2001) 194–198.
[5] C.P. Velloso, Regulation of muscle mass by growth hormone and IGF-1, Br. J. Pharmacol. 154 (2008) 557–568.
[6] N. Nagaya, M. Uematsu, M. Kojima, Y. Ikeda, F. Yoshihara, W. Shimizu, H. Hosoda, Y. Hirota, H. Ishida, H. Mori, K. Kangawa, Chronic administration of ghrelin improves left ventricular dysfunction and attenuates development of cardic cachexia in rats with heart failure, Circulation 104 (2001) 1430–1435.
[7] S. Strassburg, S.D. Anker, T.R. Castaneda, L. Burget, D. Perez-Tilve, P.T. Pfluger, R. Nogueiras, H. Halem, J.Z. Dong, M.D. Culler, R. Datta, M.H. Tschöp, Long-term effects of ghrelin and ghrelin receptor agonists on energy balance in rats, Am. J. Physiol. Endocrinol. Metab. 295 (2008) E78–E84.
[8] M. Tschöp, D.L. Smiley, M.L. Heiman, Ghrelin induces adiposity in rodents, Nature 407 (2000) 908–913.
[9] N. Nagaya, J. Moriya, Y. Yasumura, M. Uematsu, F. Ono, W. Shimizu, K. Ueno, M. Kitakaze, K. Miyatake, K. Kangawa, Effects of ghrelin administration on left ventricular function. Exercise capacity, and muscle wasting in patients with chronic heart failure, Circulation 110 (2004) 3674–3679.

[10] M.D. DeBoer, X.X. Zhu, P. Levasseur, M.M. Meguid, S. Suzuki, A. Inui, J.E. Taylor, H.A. Halem, J.Z. Dong, R. Datta, M.D. Culler, D.L. Marks, Ghrelin treatment causes increased food intake and retention of lean body mass in a rat model of cancer cachexia, Endocrinology 148 (2007) 3004–3012.
[11] M.D. DeBoer, X. Zhu, P.R. Levasseur, A. Inui, Z. Hu, G. Han, W.E. Mitch, J.E. Taylor, H.A. Halem, J.Z. Dong, R. Datta, M.D. Culler, D.L. Marks, Ghrelin treatment of chronic kidney disease: Improvements in lean body mass and cytokine profile, Endocrinology 149 (2008) 827–835.
[12] H. Ariyasu, H. Iwakura, G. Yamada, K. Nakao, K. Kangawa, T. Akamizu, Efficacy of ghrelin as a therapeutic approach for age-related physiological changes, Endocrinology 149 (2008) 3722–3728.
[13] T. Yimlamai, S.L. Dodd, S.E. Borst, S. Park, Clenbuterol induces muscle-specific attenuation of atrophy through effects on the ubiquitin–proteasome pathway, J. Appl. Physiol. 99 (2005) 71–80.
[14] S.C. Bodine, E. Latres, S. Baumhueter, V.K.-M. Lai, L. Nunez, B.A. Clarke, W.T. Poueymirou, F.J. Panaro, E. Na, K. Dharmarajan, Z.-Q. Pan, D.M. Valenzuela, T.M. DeChiara, T.N. Stitt, G.D. Yancopoulos, D.J. Glass, Identification of ubiquitin ligases required for skeletal muscle atrophy, Science 23 (2001) 1704–1708.
[15] E.T. Vestergaard, L.C. Gormsen, N. Jessen, S. Lund, T.K. Hansen, N. Moller, J.O.L. Jorgensen, Ghrelin infusion in humans induces acute insulin resistance and lipolysis independent of growth hormone signaling, Diabetes 57 (2008) 3205–3210.
[16] A.C.P. Thirone, C.R.O. Carvalho, M.J.A. Saad, Growth hormone stimulates the tyrosine kinase activity of JAK2 and induces tyrosine phosphorylation of insulin receptor substrates and Shc in rat tissues, Endocrinology 140 (1999) 55–62.
[17] N. Jessen, C.B. Djurhuus, J.O.L. Jorgensen, L.S. Jensen, N. Moller, S. Lund, O. Schmitz, Evidence against a role for insulin-signaling proteins PI 3-kinase and Akt in insulin resistance in human skeletal muscle induced by short-term GH infusion, Am. J. Physiol. Endocrinol. Metab. 288 (2005) E194–E199.
[18] M. Sandri, C. Sandri, A. Gilbert, C. Skurk, E. Calabria, A. Picard, K. Walsh, S. Sciaffino, S.H. Lecker, A.L. Goldberg, Foxo transcription factors induce the atrophy-related ubiquitin ligase atrogin-1 and cause skeletal muscle atrophy, Cell 117 (2004) 399–412.
[19] S.C. Bodine, T.N. Stitt, M. Gonzalez, W.O. Kline, G.L. Stover, R. Bauerlein, E. Zlotchenko, A. Scrimgeour, J.C. Lawrence, D.J. Glass, G.D. Yancopoulos, Akt/mTOR pathway is a crucial regulator of skeletal muscle hypertrophy and can prevent muscle atrophy in vivo, Nat. Cell Biol. 3 (2001) 1014–1019.
[20] A.S. Metlakunta, M. Sahu, A. Sahu, Hypothalamic phosphatidylinositol 3-kinase pathway of leptin signaling is impaired during the development of diet-induced obesity in FVB/N mice, Endocrinology 149 (2008) 1121–1128.
[21] M. Granado, T. Priego, A.I. Murtin, M.A. Villanua, A. Lopez-Calderon, Ghrelin receptor agonist GHRP-2 prevents arthritis-induced increase in E3 ubiquitin-ligating enzymes MuRF1 and MAFbx gene expression in skeletal muscle, Am. J. Endocrinol. Metab. 288 (2005) E1007–E1014.
[22] A. Balasubramaniam, R. Joshi, C. Su, L.A. Friend, S. Sheriff, R.J. Kagan, J.H. James, Ghrelin inhibits skeletal muscle protein breakdown in rats with thermal injury through normalizing elevated expression of E3 ubiquitin ligases MuRF1 and MAFbx, Am. J. Physiol. Regul. Integr. Comp. Physiol. 296 (2009) R893–R901.
[23] A.Z. Caron, G. Drouin, J. Desrosiers, F. Trensz, G. Grenier, A novel hindlimb immobilization procedure for studying skeletal muscle atrophy and recovery in mouse, J. Appl. Physiol. 106 (2009) 2049–2059.
[24] M. Granado, T. Priego, A.I. Murtin, M.A. Villanua, A. Lopez-Calderon, Anti-inflammatory effect of the ghrelin agonist growth hormone-releasing peptide-2 (GHRP-2) in arthritic rats, Am. J. Physiol. Endocrinol. Metab. 288 (2005) E486–E492.

Adrenomedullin: A Novel Therapy for Intractable Ulcerative Colitis

To the Editor:

In May 2010, a 68-year-old woman undergoing treatment for diabetes presented with a 3-year history of ulcerative colitis (UC). The patient was steroid-dependent, so a regimen of mesalazine (5-aminosalicylic acid [5-ASA]), prednisolone (PSL), and azathioprine (AZA) was prescribed. Despite this therapy the patient experienced a rapid deterioration, with severe abdominal pain and bloody stool (>10 times/day). Further evaluation revealed deep ulceration and erosion throughout the large intestine, which gave an Ulcerative Colitis Disease Activity Index (UCDAI) score of 12. Higher doses of PSL and AZA in combination with leukocytapheresis failed to induce remission (UCDAI score: 7). Addition of immunosuppressants or biologics was deemed unfeasible due to the patient's age, impaired glucose tolerance, and old tuberculosis, as well as the significant risk of concomitant infectious disease. After ruling out the presence of ischemic heart disease, cerebrovascular disorder, or other cardiovascular or malignant disease, adrenomedullin (AM; 1.5 pmol/kg/min) was intravenously administered for 8 hours per day for 12 days. A few days after starting the AM treatment the patient's abdominal pain and bloody stool appeared to go into remission. No adverse events were observed apart from a slight decline in blood pressure. Endoscopy at 2 weeks revealed significant mucosal regeneration (Fig. 1) and spider web-like scarring in some ulcers

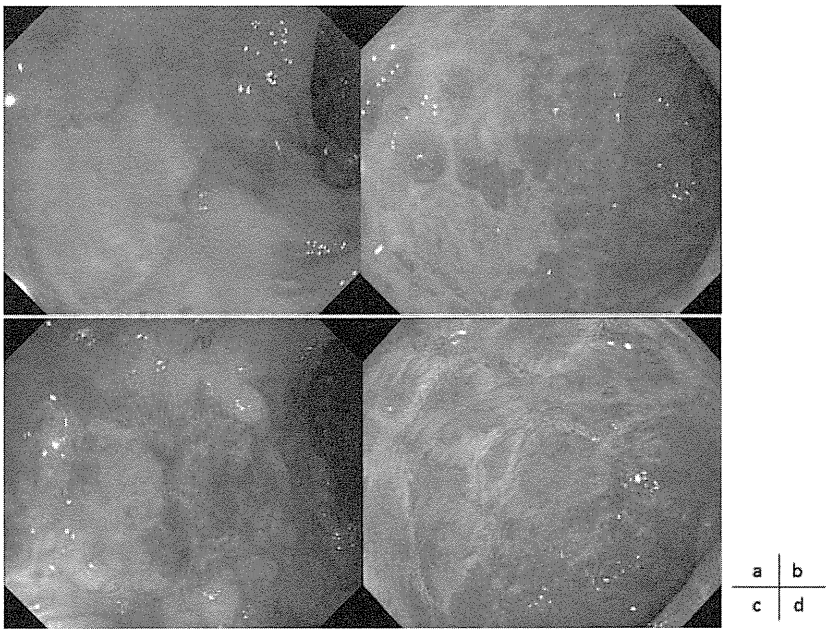

FIGURE 1. Colonoscopic findings. Wide and deep ulcers were observed in the transverse colon (a) and the sigmoid colon (b) before AM therapy. Two weeks after AM therapy (c,d), significant neovascularization and mucosal regeneration were observed at the margin and base of deep ulcers in the transverse colon (c). In the sigmoid colon, fibrosis (scarring) and vasodilation were seen in relatively shallow ulcers. Scarred regions had a reticulated, spider web-like appearance (d). [Color figure can be viewed in the online issue, which is available at wileyonlinelibrary.com.]

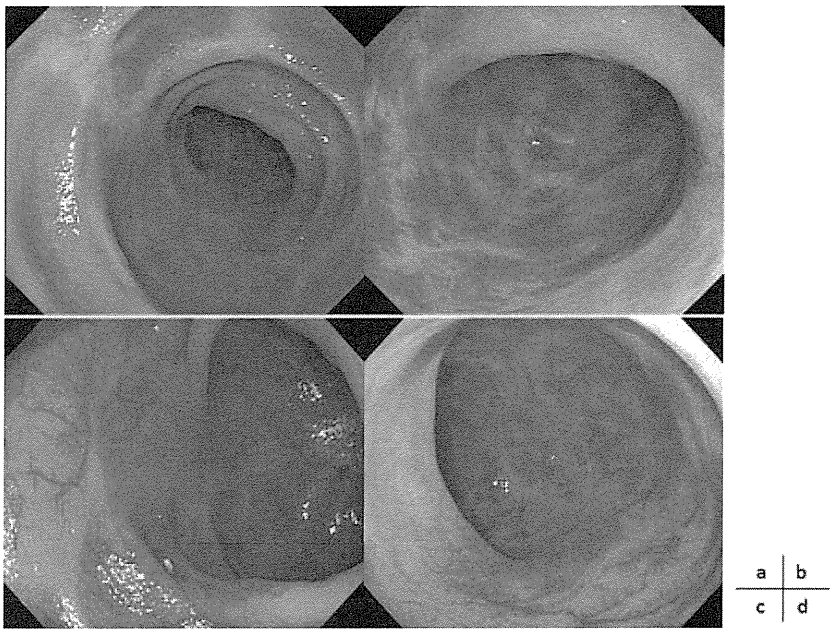

FIGURE 2. Colonoscopic findings. Three months after treatment with AM the ulcers had disappeared and ulcer scars were observed in the transverse colon (a) and the sigmoid colon (b). One year after the treatment with AM the mucosa of the transverse colon (c) and sigmoid colon (d) remained in remission without steroid therapy. [Color figure can be viewed in the online issue, which is available at wileyonlinelibrary.com.]

Supported in part by a Translational Research grant (09156271) from the Ministry of Health, Labour and Welfare of Japan.

DOI 10.1002/ibd.22891
Published online in Wiley Online Library (wileyonlinelibrary.com).

(Fig. 2), and the patient's UCDAI score had declined to 2. After 3 months, all of the patient's colonic lesions had healed with scarring and her UCDAI score had reached 0, so the PSL was discontinued.

AM was first identified as a biologically active peptide with potent vasodilating action,[1] but is now known to exert a wide range of physiological effects, including cardiovascular protection,[2] neovascularization, and suppression of inflammation and apoptosis. We previously reported that AM therapy was effective in an animal colitis model,[3] and that AM's mechanism of action is likely attributable to its suppression of inflammatory cytokines and activation of regulatory cytokines in intestinal intraepithelial lymphocytes, as well as to its protection of intercellular junctions and its antibacterial activity.[4] In addition, AM reportedly suppresses cytokine production in trinitrobenzene sulfonic acid (TNBS)-induced colitis,[5] and exerts beneficial effects on microvascular function[6] and the reepithelialization[7] of ulcers in an experimental model of colitis.

Although AM has potent hypotensive activity, we observed only minor hemodynamic effects after administering a dose of 1.5 pmol/kg/min, which we considered safe based on human dose–response data in our possession.

Conventional treatment of active UC focuses on steroids, immunosuppressants, and biologics, but the use of these drugs is restricted in geriatric and immunocompromised patients.[8] AM, on the other hand, is a physiological peptide and is therefore anticipated to have excellent safety. Here we present the first reported case in which AM was used to treat a patient with intractable UC. AM treatment produced mucosal regeneration accompanied by marked neovascularization and vasodilation visible on endoscopic examination. These findings are suggestive of AM's potential to be a ground-breaking modality with a novel mechanism of action that differs from existing immunomodulation therapy.

Shinya Ashizuka, MD, PhD
Toshihiro Kita, MD, PhD
Haruhiko Inatsu, MD
Kazuo Kitamura, MD, PhD
Division of Circulation and Body Fluid Regulation, Faculty of Medicine
University of Miyazaki
Miyazaki, Japan

REFERENCES

1. Kitamura K, Kangawa K, Kawamoto M, et al. Adrenomedullin: a novel hypotensive peptide isolated from human pheochromacytoma. *Biochem Biophys Res Commun.* 1993; 192:553–560.
2. Kataoka Y, Miyazaki S, Yasuda S, et al. The first clinical pilot study of intravenous adrenomedullin administration in patients with acute myocardial infarction. *J Cardiovasc Pharmacol.* 2010;56:413–419.
3. Ashizuka S, Ishikawa N, Kato J, et al. Effect of adrenomedullin administration on acetic acid-induced colitis in rats. *Peptides.* 2005;26: 2610–2615.
4. Ashizuka S, Inagaki-Ohara K, Kuwasako K, et al. Adrenomedullin treatment reduces intestinal inflammation and maintains epithelial barrier function in mice administered dextran sulphate sodium. *Microbiol Immunol.* 2009; 53:573–581.
5. Gonzales-Rey E, Fernandez-Martin A, Chorny A, et al. Therapeutic effect of urocortin and adrenomedullin in a murine model of Crohn's disease. *Gut.* 2006;55:824–832.
6. Talero E, Alvarez de Sotomayor M, Sánchez-Fidalgo S, et al. Vascular contribution of adrenomedullin to microcirculatory improvement in experimental colitis. *Eur J Pharmacol.* 2011;30:601–607.
7. Hayashi Y, Narumi K, Tsuji S, et al. Impact of adrenomedullin on dextran sulfate sodium-induced inflammatory colitis in mice: insights from in vitro and in vivo experimental studies. *Int J Colorectal Dis.* 2011;26:1453–1462.
8. Burger D, Travis S. Conventional medical management of inflammatory bowel disease. *Gastroenterology.* 2011;140:1827–1837.

BJP British Journal of Pharmacology

DOI:10.1111/j.1476-5381.2011.01803.x
www.brjpharmacol.org

Themed Section: Secretin Family (Class B) G Protein-Coupled Receptors – from Molecular to Clinical Perspectives

RESEARCH PAPER

The third extracellular loop of the human calcitonin receptor-like receptor is crucial for the activation of adrenomedullin signalling

Kenji Kuwasako[1], Debbie L Hay[2], Sayaka Nagata[3], Tomomi Hikosaka[3], Kazuo Kitamura[3] and Johji Kato[1]

[1]*Frontier Science Research Center, University of Miyazaki, Miyazaki, Japan,* [2]*School of Biological Sciences, University of Auckland, Auckland, New Zealand, and* [3]*Division of Circulation and Body Fluid Regulation, Faculty of Medicine, University of Miyazaki, Miyazaki, Japan*

Correspondence
Kenji Kuwasako, Frontier Science Research Center, University of Miyazaki, 5200 Kihara, Kiyotake, Miyazaki, Miyazaki 889-1692, Japan. E-mail: kuwasako@fc.miyazaki-u.ac.jp

Keywords
adrenomedullin receptor; adrenomedullin; calcitonin receptor-like receptor; extracellular loop; chimera; receptor activation; receptor activity-modifying protein

Received
11 March 2011
Revised
25 October 2011
Accepted
11 November 2011

BACKGROUND AND PURPOSE

The extracellular loops (ECLs) in Family A GPCRs are important for ligand binding and receptor activation, but little is known about the function of Family B GPCR ECLs, especially ECL3. Calcitonin receptor-like receptor (CLR), a Family B GPCR, functions as a calcitonin gene-related peptide (CGRP) and an adrenomedullin (AM) receptor in association with three receptor activity-modifying proteins (RAMPs). Here, we examined the function of the ECL3 of human CLR within the CGRP and AM receptors.

EXPERIMENTAL APPROACH

A CLR ECL3 chimera, in which the ECL3 of CLR was substituted with that of VPAC2 (a Family B GPCR that is unable to interact with RAMPs), and CLR ECL3 point mutants were constructed and transiently transfected into HEK-293 cells along with each RAMP. Cell-surface expression of each receptor complex was then measured by flow cytometry; [^{125}I]-CGRP and [^{125}I]-AM binding and intracellular cAMP accumulation were also measured.

KEY RESULTS

Co-expression of the CLR ECL3 chimera with RAMP2 or RAMP3 led to significant reductions in the induction of cAMP signalling by AM, but CGRP signalling was barely affected, despite normal cell-surface expression of the receptors and normal [^{125}I]-AM binding. The chimera had significantly decreased AM, but not CGRP, responses in the presence of RAMP1. Not all CLR ECL3 mutants supported these findings.

CONCLUSIONS AND IMPLICATIONS

The human CLR ECL3 is crucial for AM-induced cAMP responses via three CLR/RAMP heterodimers, and activation of these heterodimers probably relies on AM-induced conformational changes. This study provides a clue to the molecular basis of the activation of RAMP-based Family B GPCRs.

LINKED ARTICLES

This article is part of a themed section on Secretin Family (Class B) G Protein-Coupled Receptors. To view the other articles in this section visit http://dx.doi.org/10.1111/bph.2012.166.issue-1

Abbreviations

AM, adrenomedullin; CGRP, calcitonin gene-related peptide; CLR, calcitonin receptor-like receptor; ECL, extracellular loop; RAMP, receptor activity-modifying protein; TM, transmembrane domain

Introduction

Among the Family B GPCRs, calcitonin receptor-like receptor (CLR) is the first known partner of all three receptor activity-modifying proteins (RAMPs) (McLatchie *et al.*, 1998). When acting as chaperones, RAMPs transport CLR to the cell surface, where CLR/RAMP1 forms the functional calcitonin gene-related peptide (CGRP) receptor. CLR/RAMP2 and –3 both form adrenomedullin (AM) receptors, although CLR/RAMP2 (AM_1 receptor) is more specific for AM than CLR/RAMP3 (AM_2 receptor) (Poyner *et al.*, 2002; Hay *et al.*, 2003; Muff *et al.*, 2003). CLR/RAMP1 can also induce a similarly strong response to higher concentrations of AM (Kuwasako *et al.*, 2004a). AM, like CGRP, is a potent vasodilator that also exerts strong protective effects against multi-organ damage (Gibbons *et al.*, 2007; Kuwasako *et al.*, 2011b).

Recent crystal structural analysis revealed that activation of Family A GPCRs is accompanied by movements among the seven transmembrane domains (TMs) (Wess *et al.*, 2008; Topiol and Sabio, 2009; Simpson *et al.*, 2011; Standfuss *et al.*, 2011). A similar phenomenon is believed to also occur in Family B GPCRs (Conner *et al.*, 2007a; Chugunov *et al.*, 2010), but no crystal structure of a whole receptor is currently available. It is known from the crystal structures of Family A GPCRs that their extracellular loops (ECLs) are orientated to interact with each other and with the TMs. In addition to serving as linkers between TMs, the ECLs of Family A GPCRs are known to be important determinants of ligand binding and receptor activation (Lawson and Wheatley, 2004; Hawtin *et al.*, 2006; Peeters *et al.*, 2011). The orientation of ECL2 in the majority of Family A GPCRs is restricted by a conserved disulfide bond between ECL2 and the top of TM3 (Conner *et al.*, 2007b). Similarly, ECLs 1 and 2 in Family B GPCRs form a conserved disulfide bond for receptor stabilization (Kuwasako *et al.*, 2003). The Family B GPCR ECLs are important for peptide ligand binding and receptor activation, but little is known about the function of ECL3, and there have been no reports on the function of TMs 1, 2, 4, 5 and 7 of CLR (Walker *et al.*, 2010; Wheatley *et al.*, 2012).

As with Family A GPCRs, the functions of the various regions of Family B GPCRs have been investigated using a chimeric receptor strategy, in which the target sequence of one GPCR was replaced with the corresponding sequence from a different GPCR (Nielsen *et al.*, 2000; Van Rampelbergh *et al.*, 2000; Unson *et al.*, 2002; Runge *et al.*, 2003; Koller *et al.*, 2004; Salvatore *et al.*, 2006; Kuwasako *et al.*, 2009). To determine which structural regions of human (h)CLR govern CLR/RAMP trafficking and function, we recently generated a set of nine chimeras (CH-1 to CH-9) in which regions of CLR were replaced with corresponding sequences from vasoactive intestinal peptide (VIP)/pituitary adenylate cyclase-activating polypeptide type 2 receptor (VPAC2; another Family B GPCR), which does not interact with RAMPs (Christopoulos *et al.*, 2003). Using these chimeras, we first determined the CLR regions (between TM1 and TM5) responsible for the trafficking interactions with each RAMP (Kuwasako *et al.*, 2009). Our preliminary experiments showed that CH-7, which contained ECL3 and TM7 from VPAC2, impaired the production of cAMP by AM via the AM_1 and AM_2 receptors but affected CGRP responses via the CGRP receptor to a lesser extent.

To investigate the function of the CLR ECL3 within the CGRP and AM receptors, we generated CH-I and CH-II, in which the ECL3 and TM7 of CLR were each substituted with the corresponding sequences from VPAC2. Our findings suggest that the CLR ECL3 plays a key role in AM-induced cAMP signalling via the three CLR/RAMP heterodimers, and the activation of these heterodimers probably relies on AM-induced conformational changes.

Methods

Expression constructs

Double V5 epitope-tagged human CLR (V5-CLR) and all three V5-RAMPs were prepared as described previously (Kuwasako *et al.*, 2009) and cloned into the mammalian expression vector pCAGGS/Neo (Kuwasako *et al.*, 2000). Corresponding untagged constructs served as controls.

Chimera construction

We previously used seven restriction sites to construct nine human CLR chimeras (CH-1 to CH-9), in which CLR domains were sequentially substituted with corresponding sequences from the human VPAC2 receptor (Kuwasako *et al.*, 2009). Of those chimeras, CH-7, in which the ECL3 and TM7 of CLR were exchanged with those of VPAC2, was used in the present study (Figure 1). As shown in Figure 1B, we also constructed two new CLR/VPAC2 chimeras, CH-I and CH-II, in which either CLR ECL3 or TM7 was replaced with the corresponding sequence from VPAC2 using three restriction sites *Eco*T14 I (*Sty* I), *Eco*T22 I (*Ava* III) and *Avi* II (*Mst* I). Human CLR naturally possesses an *Eco*T14 I site, and the other two sites were introduced without altering the amino acid sequence of the receptor. Human VPAC2 shares only 30% amino acid sequence identity with human CLR and contains none of the three restriction sites. Therefore, corresponding VPAC2 fragments containing the necessary restriction sites were prepared by PCR using a primer set containing the sites 5′-*Eco*T14 I-VPAC2 ECL3-*Eco*T22 I-3′ and 5′-*Eco*T22 I-VPAC2 TM7-*Avi* II-3′. The separate CLR and VPAC2 fragments were then ligated into the same pCAGGS/Neo expression vector. The resulting chimeric constructs were all sequenced using an Applied Biosystems 310 Genetic Analyzer (Foster City, CA, USA).

Site-directed mutagenesis

Single and triple amino acid substitutions were carried out using a QuikChange kit (Stratagene Corporation, La Jolla, CA, USA) according to the manufacturer's instructions, with pIRES1-V5-CLR serving as the template. pIRES1-V5-CLR was constructed by subcloning the coding sequence of human V5-CLR into pIRES/Neo (Clontech, Palo Alto, CA). For each mutation, two complementary 30- to 40-mer oligonucleotides (sense and antisense) were designed with the mutation in the middle. The resulting mutants were all sequenced using an Applied Biosystems 310 Genetic Analyzer.

Cell culture and DNA transfection

HEK-293 cells were maintained in Dulbecco's modified Eagle medium (DMEM) supplemented with 10% heat-inactivated

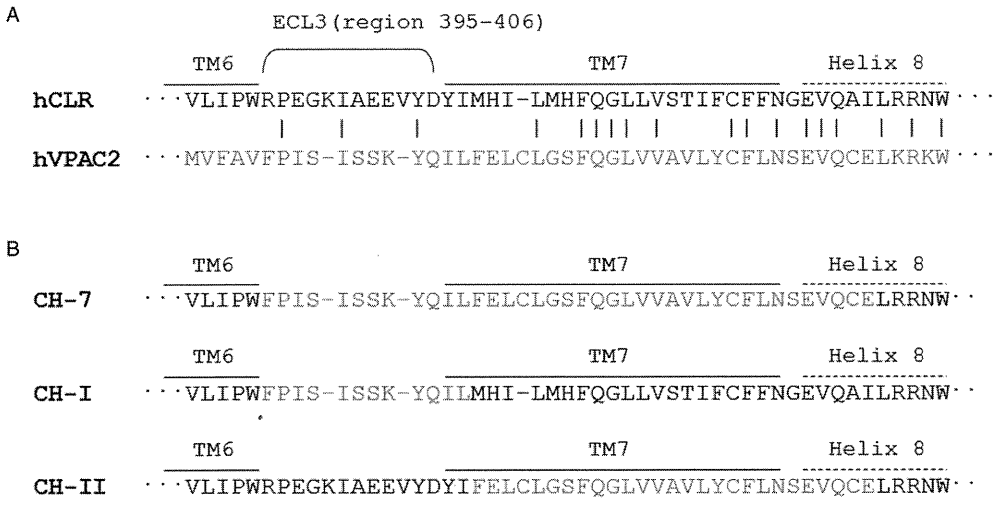

Figure 1

(A) Amino acid sequence alignment of ECL3 and TM7 of human CLR with the corresponding domains of the human VPAC2 receptor. Alignment of CLR ECL3 and TM7 is based on a previous report (Bailey and Hay, 2007). A homology search for both receptors was performed using DNASIS (Hitachi Solutions, Ltd, Tokyo, Japan). Vertical dashes indicate conserved amino acids. (B) Alignment of the three CLR/VPAC2 chimeras. Chimeras were constructed using three restriction sites: *Eco*T14 I, *Eco*T22 I and *Avi* II (see Methods section). CH-7 was generated by replacing CLR ECL3 and TM7 with the corresponding sequence from VPAC2 using 5′ *Eco*T14I and 3′ *Avi* II sites (Kuwasako *et al.*, 2009). Likewise, CH-I and CH-II were constructed by substituting CLR ECL3 (using 5′ *Eco*T14 I and 3′ *Eco*T22 I sites) or CLR TM7 (using 5′ *Eco*T22 I and 3′ *Avi* II sites), respectively.

fetal bovine serum (FBS), 100 U·mL^{-1} penicillin G, 100 μg·mL^{-1} streptomycin and 0.25 μg·mL^{-1} amphotericin B at 37°C under a humidified atmosphere of 95% air/5% CO_2. Transient transfection of the cells was accomplished using Lipofectamine™ with Plus™ reagent (Invitrogen Corporation, Carlsbad, CA, USA) as previously described (Kuwasako *et al.*, 2011a). Briefly, the cells were seeded into 12-well plates (for flow cytometric analysis) or 24-well plates (for binding and cAMP assays) and, upon reaching 70–80% confluence, were transfected with empty vector (pCAGGS/Neo or pIRES/Neo) (*Mock*) or V5-tagged wild-type (WT), pCAGGS-chimeric or pIRES-mutant constructs; V5-CLR was included in each transfection set. DNA complex with transfection reagents was formed by incubating the cells for 4 h in OptiMEM 1 medium containing plasmid DNAs (0.2 μg per well for 24-well plates; 0.4 μg per well for 12-well plates), Plus reagent (2 μL per well for 24-well plates; 2.5 μL per well for 12-well plates) and Lipofectamine reagent (2 μL per well for 24-well plates; 2.5 μL per well for 12-well plates). All experiments were performed 36–48 h after transfection.

Flow cytometry

Flow cytometry was used to assess the cell-surface expression levels of V5-tagged receptor proteins. Following transient co-transfection of the indicated cDNAs for WT or mutant V5-CLR and RAMP or those for WT or mutant CLR and V5-RAMP into HEK-293 cells in 12-well plates, the cells were washed once with ice-cold PBS and then non-enzymatically harvested with ice-cold FACS buffer (Kuwasako *et al.*, 2000). After centrifugation at 200× *g* for 4 min at 4°C, the cells were resuspended in FACS buffer and labelled with fluorescein isothiocyanate (FITC) conjugated mouse anti-V5 monoclonal antibody (anti-V5-FITC antibody) (Invitrogen, diluted 1:1000 in FACS buffer) for 2 h at 4°C in the dark. The cells were then washed twice with ice-cold FACS buffer, resuspended to a density of 2×10^5 cells per tube in FACS buffer containing 5 μg·mL^{-1} propidium iodide and subjected to flow cytometry in an EPICS XL flow cytometer (Beckman Coulter, Fullerton, CA, USA). The cell-surface expression frequency of each V5-tagged receptor (% of cells) was analysed using EXPO 2 software (Beckman Coulter) (Kuwasako *et al.*, 2000). FITC fluorescence was excited at 488 nm, and emission was monitored at 530 nm. Viability was assessed on the basis of the exclusion of propidium iodide.

Radioligand binding

[^{125}I]-[His^{10}]-αCGRP (specific activity 2.2 μCi·pmol^{-1}) was purchased from PerkinElmer (Yokohama, Japan), and [^{125}I]-AM (specific activity 2 μCi·pmol^{-1}) was produced in our laboratory as previously described (Kitamura *et al.*, 1994). To assess whole-cell radioligand binding, transfected HEK-293 cells in 24-well plates were washed once with pre-warmed PBS and incubated for 20 min at 37°C with 0.1% BSA/PBS to reduce non-specific binding of αCGRP and AM, after which, the remaining adherent cells were washed with ice-cold PBS. The cells were then incubated with 40 000 c.p.m. of [^{125}I]-αCGRP or 100 000 c.p.m. of [^{125}I]-AM for 4 h at 4°C in the absence (for total binding) or presence of different concentrations of unlabelled αCGRP or AM as appropriate (1 μM was used to define non-specific binding) in modified Krebs-Ringers-HEPES medium (Kuwasako *et al.*, 2000). After washing once with ice-cold PBS, the cells were solubilized with 0.5 mL of 0.5 M NaOH, and the associated cellular radioactivity was measured in a γ-counter. Specific binding was defined as the difference between the total binding and non-specific binding.

Measurement of intracellular cAMP

cAMP assays were carried out as described previously (Kuwasako *et al.*, 2011a). Transfectants in 24-well plates were incubated for 15 min at 37°C in Hanks' buffer containing 20 mM HEPES, 0.2% BSA, 0.5 mM 3-isobutyl-1-methylxanthine (IBMX) and the indicated concentrations of AM. The reactions were terminated by the addition of lysis buffer (GE Healthcare, Tokyo, Japan), after which, the cAMP content was determined using a commercial enzyme immunoassay kit according to the manufacturer's instructions (GE Healthcare) for a non-acetylation protocol.

Data analysis and statistics

At least five independent replicates were performed for each of the aforementioned experiments, and the results are expressed as mean ± SEM. Data were analysed using Prism 5.02 (GraphPad Software Inc., San Diego, CA, USA). The binding and cAMP data were fitted to obtain pIC_{50} and pEC_{50} values, respectively. A four-parameter logistic equation was used for curve fitting. For each fit, the Hill slope was compared to unity by *F*-test. When the Hill slope was not different from one, the data were re-fitted to a three-parameter logistic equation (Hill slope of one). In cases where the Hill slope differed from one, further analysis was performed to ascertain whether Hill slopes differed within a particular data set by *F*-test. Hill slopes that deviate from unity are reported within the results narrative. Differences among multiple groups were evaluated using one-way ANOVA as appropriate, where $P < 0.05$ was considered significant. *Post hoc* testing was via Dunnett's test for comparison with control.

Reagents and other materials

All ^{125}I-labelled and unlabelled ligands used were of human origin. αCGRP was purchased from the Peptide Institute (Osaka, Japan), and AM was kindly donated by Shionogi & Co. (Osaka, Japan). Peptides were dissolved in sterile, distilled H_2O to a concentration of 1 mM and stored as aliquots at –80°C in siliconized microcentrifuge tubes. IBMX and BSA were from Sigma-Aldrich Corporation (St Louis, MO, USA). DMEM and FBS were from Invitrogen. All other reagents were of analytical grade and obtained from various commercial suppliers.

Results

Cell-surface expression of CLR/VPAC2 chimeras co-expressed with RAMPs

We initially evaluated the effects of transient co-transfection of WT-RAMPs on the cell-surface expression of V5-CH-7, V5-CH-I and V5-CH-II in HEK-293 cells (Figure 2A), which do not endogenously express any functional CGRP or AM receptors (Kuwasako *et al.*, 2004b; 2008). In cells transfected with the empty vector (Mock), surface binding of an anti-V5-FITC antibody was within the 2% limit of resolution characteristic of flow cytometry. When expressed alone, FITC-labelled V5-CLR was detected in ~30% of cells. This phenomenon has also been seen in COS-7 cells, which are frequently used in transfection studies and also express no functional RAMPs

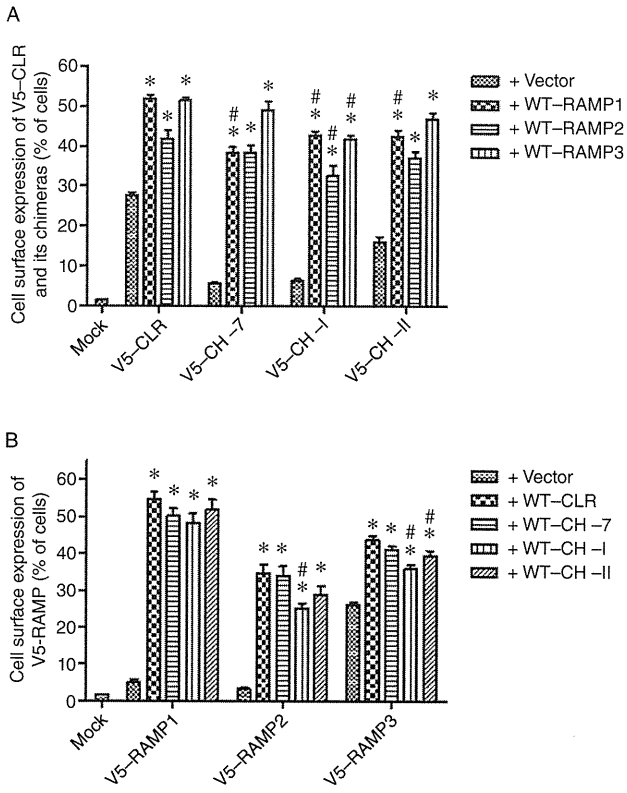

Figure 2

(A) Flow cytometric analysis of the cell-surface expression of WT or chimeric V5-CLR (CH-7, CH-I and CH-II) following transfection into HEK-293 cells, with or without WT-RAMP1, -2 or -3. Cell-surface expression of each FITC-labelled receptor protein was estimated by flow cytometry. Data are shown as the means ± SEM of five separate experiments. $^*P < 0.05$ vs. corresponding Vector/V5-CLR or -CH, $^{\#}P < 0.05$ vs. corresponding V5-CLR/WT-RAMP. (B) Flow cytometric analysis of the cell-surface expression of V5-RAMP1, -2 or -3 following transfection into HEK-293 cells, with WT or chimeric CLR (CH-7, CH-I and CH-II). Cell-surface expression of each construct was analysed by flow cytometry. Data are shown as the means ± SEM of six separate experiments. $^*P < 0.05$ vs. corresponding Vector/V5-RAMP, $^{\#}P < 0.05$ vs. corresponding WT-CLR/V5-RAMP.

(Ittner *et al.*, 2004; Koller *et al.*, 2004; Kuwasako *et al.*, 2009). In the present study, the frequency of surface WT V5-CLR and chimeric V5-CLR expression was significantly increased by the co-transfection of each RAMP. In the absence of exogenous RAMPs, two chimeras, CH-7 and CH-I, appeared at the cell surface at levels nearly the same as that seen with Mock. We compared the expression of each chimera to WT, when expressed with each RAMP. With RAMP1, each chimera caused a small but significant decrease in cell-surface delivery, compared to WT. For RAMP2 and RAMP3, only CH-I delivery was slightly reduced.

We also assessed the changes in the frequency of cell-surface expression of V5-RAMPs that occurred after co-transfection of untagged WT and chimeric CLR (Figure 2B). In contrast to V5-RAMP1 and V5-RAMP2, V5-RAMP3 appeared at the surface of ~28% of cells when the protein was expressed alone, probably because of its self-

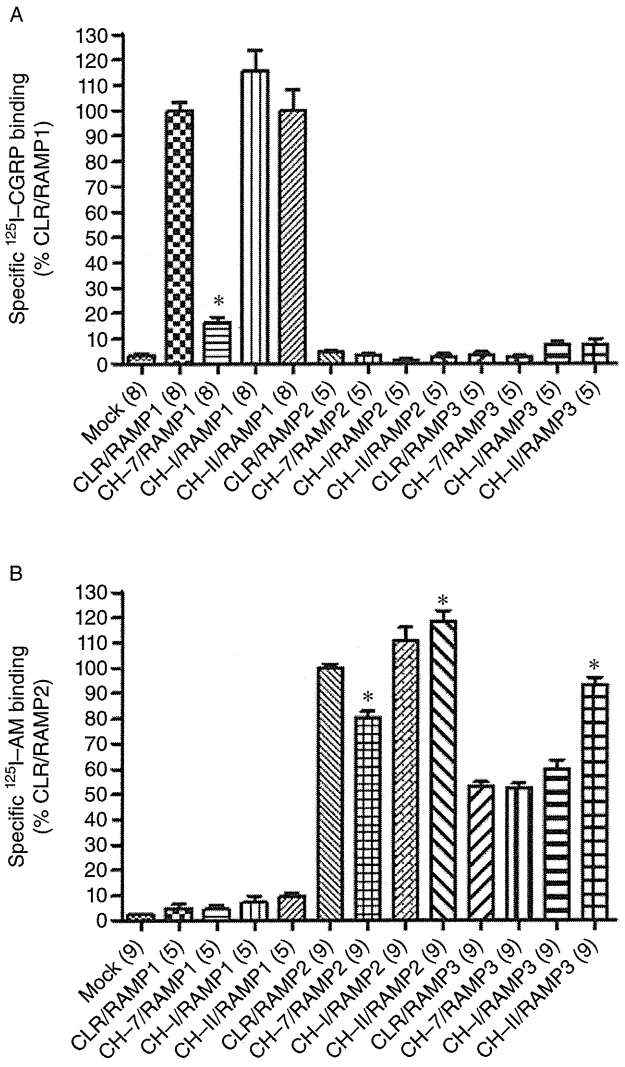

Figure 3

Specific binding of [^{125}I]-CGRP (A) and [^{125}I]-AM (B) to heterodimeric receptors composed of WT-RAMP and WT or chimeric CLR (CH-7, CH-I and CH-II). HEK-293 cells were transiently transfected with a WT-RAMP and WT-CLR or one of its three chimeras. Data are shown as the means ± SEM of five to eight experiments in (A) and five to nine experiments in (B) and are expressed as percentages of CLR/RAMP1 (A) or CLR/RAMP2 (B). *$P < 0.05$ vs. corresponding WT-CLR/RAMP (A, B).

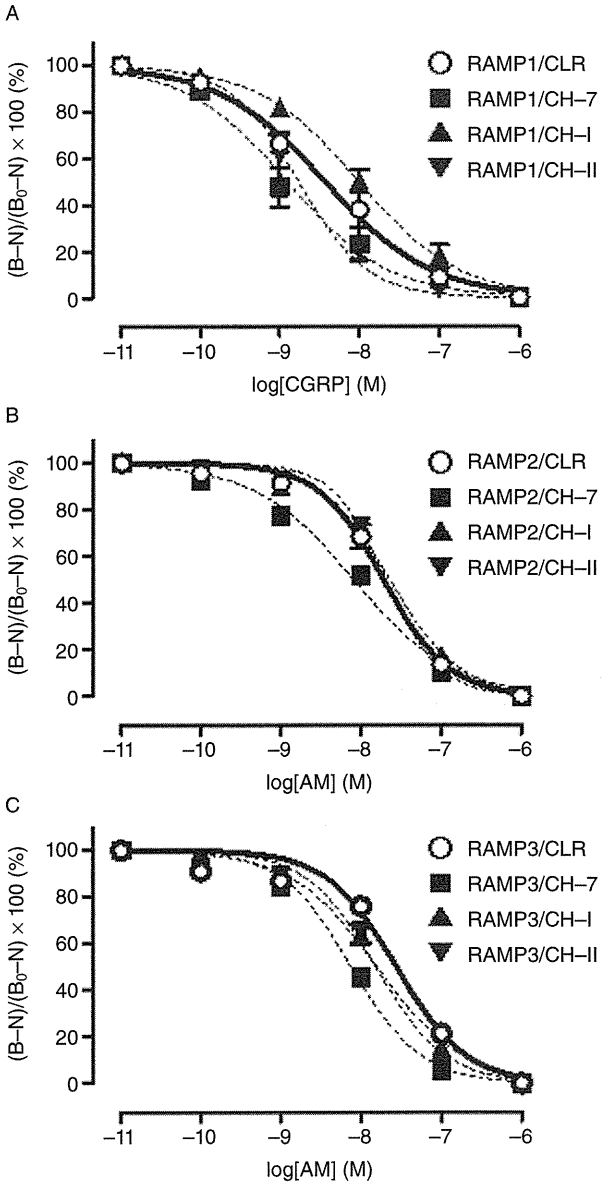

Figure 4

Competitive binding of [^{125}I]-CGRP to WT or chimeric CLR/RAMP1 (A) and binding of [^{125}I]-AM to WT or chimeric CLR/RAMP2 (B) or CLR/RAMP3 (C). HEK-293 cells were transiently co-transfected with each WT-RAMP and WT or chimeric CLR (CH-7, CH-I and CH-II). Data were normalized to the maximum specific binding in each experiment. Data are shown as the means ± SEM of five experiments in (A, C) and six experiments in (B). (B) Binding of [^{125}I]-CGRP (A) or [^{125}I]-AM (B, C); B_o, total binding in the presence of competing unlabelled CGRP (A) or AM (B, C); N, nonspecific binding (measured in the presence of 10^{-6} M CGRP (A) or 10^{-6} M AM (B, C)). pIC_{50} values are given in Table 1.

transport to the cell surface (Flahaut *et al.*, 2002) or its interaction with other endogenous GPCRs (Hay *et al.*, 2006; Sexton *et al.*, 2009). CH-7, CH-I and CH-II all markedly increased the frequency of the surface expression of V5-RAMP1 and V5-RAMP2 to a level comparable to that seen with CLR. Significant increases in V5-RAMP3 translocation were also observed when it was co-expressed with the WT or chimeric CLR constructs, but the magnitude of the changes was much smaller than was seen with V5-RAMP1 and V5-RAMP2. The expression frequency of RAMP1 was unchanged in the presence of each chimera when compared to WT. A significant decrease in RAMP2 and RAMP3 expression was observed in the presence of CH-I. CH-II only reduced the expression of RAMP3.

[125I]-CGRP and [125I]-AM binding to cell-surface CLR/VPAC2 chimeras

We next evaluated the binding of [125I]-CGRP and [125I]-AM to cells expressing each of the WT and chimeric receptors (Figures 3 and 4). Cells transfected with Mock showed only low levels of specific radioligand binding (Figure 3), but marked increases in [125I]-CGRP binding were observed in cells expressing RAMP1 with WT-CLR, CH-I or CH-II (Figure 3A). The specific binding of [125I]-CGRP to CH-7/RAMP1 was also increased but was much lower than the binding to CH-I/RAMP1 and CH-II/RAMP1. Cells co-expressing RAMP2 or RAMP3 with WT-CLR or one of the chimeras bound little [125I]-CGRP. In contrast, marked increases in specific [125I]-AM binding were seen with all four CLR proteins co-expressed with RAMP2 or RAMP3 (Figure 3B). There was no significant difference between the specific [125I]-AM binding to CH-I/RAMP2 and CLR/RAMP2. However, the specific binding of [125I]-AM to CH-7/RAMP2 was significantly lower than to CLR/RAMP2, while the specific binding of [125I]-AM to CH-II/RAMP2 was significantly higher than to CLR/RAMP2. CLR/RAMP3 exhibited a lower level of specific [125I]-AM binding than CLR/RAMP2, which is consistent with earlier observations (Kuwasako *et al.*, 2006). Interestingly, the specific binding of [125I]-AM to CH-II/RAMP3 was about twofold higher than was seen with the other three RAMP3/CLR proteins. Figure 4 shows [125I]-CGRP and [125I]-AM competition curves for the WT and chimeric receptors. The pIC_{50} values derived from the curves are given in Table 1. CH-7/RAMP1 (Hill slope = 0.68) and CH-II/RAMP1 exhibited significantly higher CGRP affinity than CLR/RAMP1 (Hill slope = 0.64), whereas the affinity of CGRP for CH-I/RAMP1 (Hill slope = 0.69) was significantly lower than that for CLR/RAMP1. Although some of the Hill slopes for these curves deviated from unity, they were not different from each other. CH-7/RAMP2 (Hill slope = 0.70) exhibited significantly higher AM affinity than CLR/RAMP2, but the affinity of AM for CH-I/RAMP2 and CH-II/RAMP2 (Hill slope = 1.29) was similar to that for CLR/RAMP2. In the case of this RAMP2 data set, the Hill slopes were different between chimeras and WT. The affinity of AM was significantly increased at CH-7/RAMP3, CH-I/RAMP3 (Hill slope = 0.81) and CH-II/RAMP3 relative to CLR/RAMP3.

Table 1

pIC_{50} values for CGRP in competition with [125I]-CGRP binding to RAMP1/WT or chimeric CLR and for AM in competition with [125I]-AM binding to RAMP2/WT or chimeric CLR and RAMP3/WT or chimeric CLR

Receptor complex	pIC_{50} ± SEM	*n*
RAMP1/WT-CLR	8.43 ± 0.07	5
RAMP1/CH-7	8.91 ± 0.10*	5
RAMP1/CH-I	8.01 ± 0.06*	5
RAMP1/CH-II	8.76 ± 0.08*	5
RAMP2/WT-CLR	7.72 ± 0.04	6
RAMP2/CH-7	8.09 ± 0.05*	6
RAMP2/CH-I	7.64 ± 0.04	6
RAMP2/CH-II	7.68 ± 0.02	6
RAMP3/WT-CLR	7.56 ± 0.06	5
RAMP3/CH-7	8.13 ± 0.04*	5
RAMP3/CH-I	7.80 ± 0.05*	5
RAMP3/CH-II	7.81 ± 0.04*	5

*$P < 0.05$ vs. the corresponding RAMP/WT-CLR one-way ANOVA followed by Dunnett's multiple comparison test.
RAMP, receptor activity-modifying protein; WT, wild-type; CLR, calcitonin receptor-like receptor; CGRP, calcitonin gene-related peptide; AM, adrenomedullin; CH, chimera.

CGRP- and AM-induced cAMP production via CLR/VPAC2 chimeras

The three chimeric receptors were further characterized by measuring agonist-induced cAMP accumulation (Figure 5). Their pEC_{50} and E_{max} values are given in Table 2. As previously reported (Kuwasako *et al.*, 2009), neither CGRP nor AM elicited cAMP production in HEK-293 cells transfected with Mock (data not shown).

When co-expressed with RAMP1, there were no significant decreases in the pEC_{50} and E_{max} values for CGRP with CH-I or CH-II compared with WT-CLR (Figure 5A, C and D). That is, CGRP was able to activate all three RAMP1-associated receptors with similar potency and efficacy. In contrast, CGRP acting via CH-7/RAMP1 showed an approximately 60-fold reduction in potency with no significant reduction in efficacy (Figure 5B). Recombinant CLR/RAMP1 can also respond fully to higher concentrations of AM (Kuwasako *et al.*, 2004a). In cells expressing CLR/RAMP1, the potency of AM was about 60-fold lower than that of CGRP (Figure 5A). Although the potency of CGRP and AM for CH-II/RAMP1 was not significantly different from that for CLR/RAMP1 (Table 2, Figure 5D), CH-7/RAMP1 significantly reduced the potency of each agonist (Figure 5B). Surprisingly, in cells expressing CH-I/RAMP1, the potency of AM was about 460-fold lower than that of CGRP, despite the fact that CH-I/RAMP1 mediated CGRP-induced cAMP responses normally (Figure 5C). For AM potency, only the Hill slope (0.63) of CH-II/RAMP1 differed from 1.

In cells expressing CLR/RAMP2 (AM_1 receptor), the potency of AM was about 210-fold higher than that of CGRP (Figure 5E), while in cells expressing CLR/RAMP3 (AM_2 receptor), the potency of AM was about 100-fold higher (Figure 5I). Cells expressing RAMP2 with CH-7 or CH-I showed marked reductions in AM potency and efficacy (Figure 5F and G). The potency of AM with CH-7/RAMP2 and CH-I/RAMP2 was reduced by about 60-fold and 100-fold, respectively, and the efficacy was reduced by about 80% and 50% compared with the WT AM_1 receptor (Figure 5F and G). Most notably, CH-I/RAMP2 exhibited normal [125I]-AM binding (Figure 3B and Table 1). On the other hand, the potency of AM for CH-7/RAMP3 and CH-I/RAMP3 was decreased by about 15-fold and 20-fold, respectively, and the efficacy was decreased by about 40% and 30% compared with the WT AM_2 receptor (Figure 5J and K). In contrast, the efficacy of AM with CH-II/RAMP2 and CH-II/RAMP3 was not significantly different from that for WT AM_1 and AM_2 receptors, respectively (Figure 5H and L), although the AM potency for CH-II/RAMP2 and the CGRP potency for CH-II/RAMP3 were significantly reduced relative to each WT AM

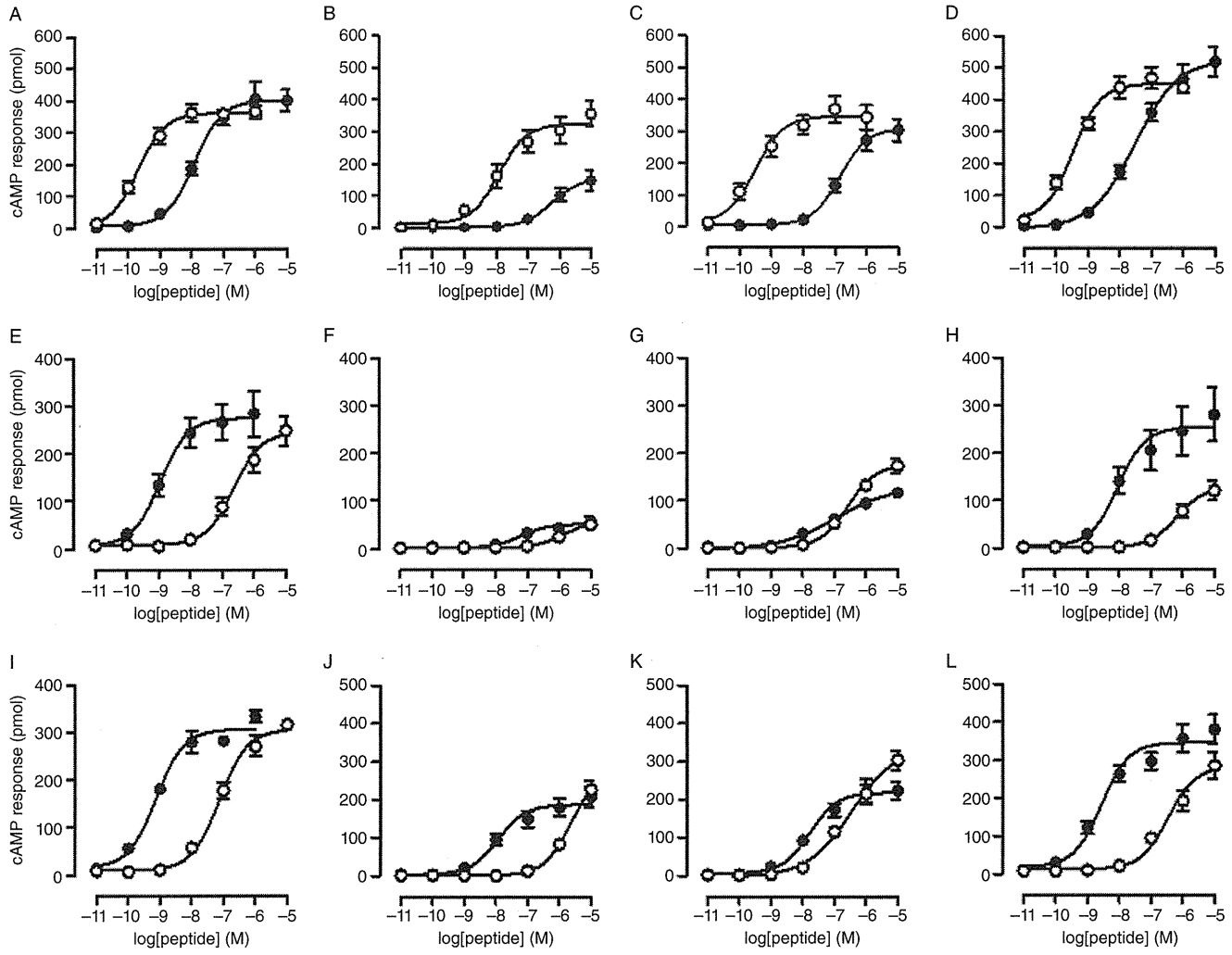

Figure 5

Agonist-induced cAMP production elicited via heterodimeric receptors comprised of WT-RAMP and WT or chimeric CLR (CH-7, CH-I and CH-II). HEK-293 cells were co-transfected with WT-RAMP1 plus WT-CLR (A), CH-7 (B), CH-I (C) or CH-II (D); WT-RAMP2 plus WT-CLR (E), CH-7 (F), CH-I (G) or CH-II (H); or WT-RAMP3 plus WT-CLR (I), CH-7 (J), CH-I (K) or CH-II (L). All transfected cells (A–L) were simultaneously exposed to the indicated concentrations of αCGRP (open symbols) or AM (solid symbols) 48 h after transfection. Data are shown as the means ± SEM of five separate experiments. pEC_{50} values are given in Table 2.

receptor. Among these RAMP2- and RAMP3-based receptors, only the Hill slopes of CH-I/RAMP2 (0.49 for AM) and CH-I/RAMP3 (0.62 for CGRP) were different from 1.

Further investigation of the function of CLR ECL3 in AM receptors

The data summarized earlier indicate that among the three CLR/VPAC2 chimeras tested, co-transfection of CH-7 with RAMP1, RAMP2 or RAMP3 leads to marked decreases in CGRP and AM responses. CH-I had marked effects on responses to AM in the presence of each RAMP, despite appropriate [^{125}I]-AM binding and surface delivery. In contrast, CH-I had little effect on CGRP potency or efficacy. CH-II/RAMP1 maintained full CGRP receptor function, whereas CH-II/RAMP2 and CH-II/RAMP3 exhibited small but significant reductions in CGRP/AM potency. These findings indicate that the CLR ECL3 is crucial for AM signalling via the CGRP, AM_1 and AM_2 receptors, but it is less critical for CGRP signalling via these three receptors. We therefore constructed four mutants (Mut-A, Mut-B, Mut-C and Mut-D) in which CLR ECL3 residues with no homology to VPAC2 were sequentially replaced with alanine (Ala) (Figure 6); the effects of these mutants were characterized following transient transfection.

As with WT-CLR, all four CLR mutants were increased at the cell surface, even when expressed alone (Figure 7A). The cell-surface expression of these four mutants was significantly increased by co-transfection with WT-RAMP1, WT-RAMP2 or WT-RAMP3 to such an extent that their expression frequen-

Table 2

Agonist-induced cAMP response in cells co-expressing RAMP with WT or chimeric CLR

Receptor complex	CGRP pEC_{50}	CGRP E_{max} (pmol)	AM pEC_{50}	AM E_{max} (pmol)
RAMP1/WT-CLR	9.70 ± 0.13	361.5 ± 11.1	7.92 ± 0.13	400.7 ± 16.8
RAMP1/CH-7	7.93 ± 0.18*	325.7 ± 18.7	6.29 ± 0.23*	154.3 ± 17.0*
RAMP1/CH-I	9.50 ± 0.22	345.7 ± 18.2	6.84 ± 0.13*	308.3 ± 16.3*
RAMP1/CH-II	9.47 ± 0.13	450.3 ± 14.0*	7.52 ± 0.16	526.6 ± 32.3*
RAMP2/WT-CLR	6.63 ± 0.16	244.9 ± 16.0	8.95 ± 0.22	274.7 ± 18.2
RAMP2/CH-7	5.85 ± 0.13*	57.7 ± 4.4*	7.19 ± 0.26*	51.6 ± 4.9*
RAMP2/CH-I	6.57 ± 0.10	174.6 ± 7.7*	6.93 ± 0.24*	129.5 ± 13.7*
RAMP2/CH-II	6.18 ± 0.16	128.9 ± 11.1*	8.03 ± 0.26*	253.7 ± 21.1
RAMP3/WT-CLR	7.13 ± 0.08	305.5 ± 9.4	9.12 ± 0.10	306.3 ± 8.8
RAMP3/CH-7	5.62 ± 0.10*	281.5 ± 18.5	7.94 ± 0.18*	187.9 ± 10.7*
RAMP3/CH-I	6.46 ± 0.21*	338.7 ± 36.0	7.78 ± 0.16*	218.9 ± 11.0*
RAMP3/CH-II	6.46 ± 0.15*	283.2 ± 18.7	8.56 ± 0.16*	346.6 ± 14.4

*$P < 0.05$ vs. the corresponding RAMP/WT-CLR, one-way ANOVA followed by Dunnett's multiple comparison test.
Data are displayed as the means ± SEM of five independent experiments.
E_{max} values are the maximum asymptote of concentration-effect curves and correspond to the amount of cAMP.
RAMP, receptor activity-modifying protein; WT, wild-type; CLR, calcitonin receptor-like receptor; CGRP, calcitonin gene-related peptide; AM, adrenomedullin; CH, chimera.

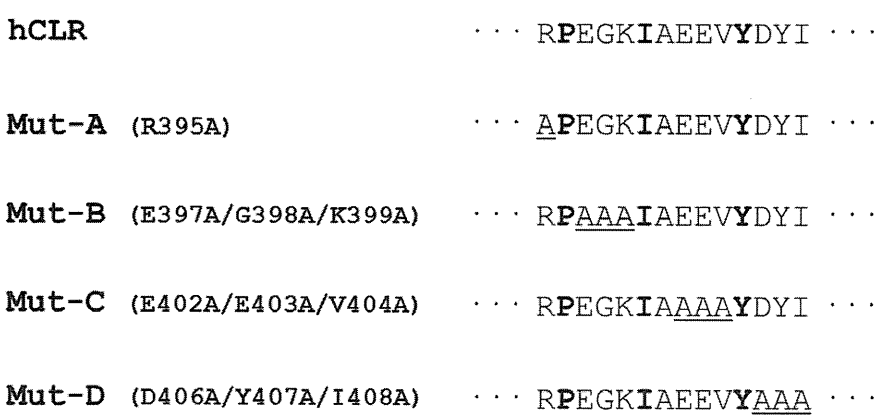

Figure 6

Amino acid sequence alignment of the human CLR chimera CH-7 and alanine substitutions in the region spanning amino acids 395–408. Note that the region contains CLR ECL3 (amino acids 395–406). Bold letters indicate amino acid residues (Pro, Ile and Tyr) conserved between CLR and VPAC2. Residues that are not conserved were sequentially replaced with alanine (A): mutant (Mut)-A (R395A), Mut-B (E397A + G398A + K399A), Mut-C (E402A + E403A + V404A) and Mut-D (D406A + Y407A + I408A).

cies were not significantly different from those of the corresponding V5-CLR/RAMP (Figure 7A). All four untagged mutants markedly increased the translocation of V5-RAMP1, V5-RAMP2 or V5-RAMP3 to a level comparable to that seen with WT-CLR (Figure 7B).

Figure 7C and D shows the specific binding of [^{125}I]-CGRP and [^{125}I]-AM to the WT and mutant receptors for CGRP or AM. The specific [^{125}I]-CGRP binding to Mut-A/RAMP1 was significantly greater than to the WT CGRP receptor, whereas the remaining three mutant receptors exhibited specific [^{125}I]-CGRP binding comparable to the WT CGRP receptor (Figure 7C). Likewise, the specific binding of [^{125}I]-AM to Mut-A/RAMP2 was significantly greater than to the WT AM_1 receptor. The specific binding of [^{125}I]-AM to the remaining three mutant receptors was similar to the binding to the WT AM_1 receptor (Figure 7D). There were also no significant differences in specific [^{125}I]-AM binding to the WT and mutant AM_2 receptors (Figure 7D). [^{125}I]-CGRP and [^{125}I]-AM competition curves for WT and mutant receptors are shown in Figure 8A–C. The pIC_{50} values

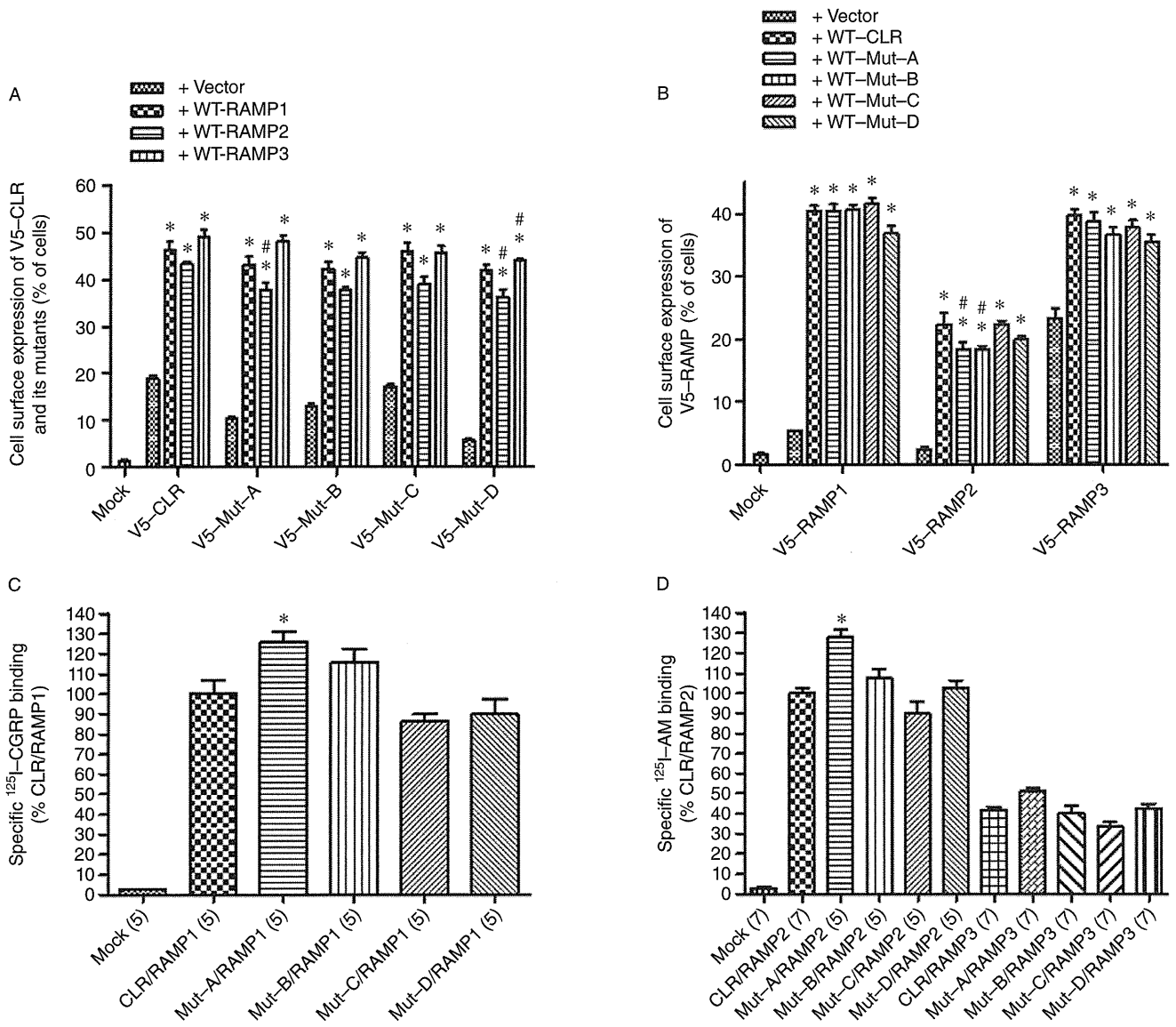

Figure 7

Effect of CLR ECL3 point mutations on cell-surface expression and specific binding of agonists. (A) Cell-surface expression of V5-tagged WT or mutant CLR. WT-CLR or one of four CLR mutants (Mut-A, -B, -C and -D) was transiently transfected into HEK-293 cells, with or without WT-RAMP. The cell-surface expression of each FITC-labelled protein was estimated by flow cytometry. Data are means ± SEM of five to eight separate experiments. $^{*}P < 0.05$ vs. corresponding Vector/V5-CLR or –Mut, $^{\#}P < 0.05$ vs. corresponding V5-CLR/WT-RAMP. (B) Changes in the cell-surface expression of V5-RAMP induced by co-transfection with WT or mutant CLR (Mut-A, -B, -C and -D). The indicated constructs were transfected into HEK-293 cells, after which the cell-surface expression of each V5-tagged protein was analysed by flow cytometry. Data are shown as the means ± SEM of five to nine separate experiments. $^{*}P < 0.05$ vs. corresponding Vector/V5-RAMP, $^{\#}P < 0.05$ vs. corresponding WT-CLR/V5-RAMP. (C and D) Specific binding of [^{125}I]-CGRP (C) and [^{125}I]-AM (D) to heterodimeric receptors composed of WT RAMP and WT or mutant CLR (Mut-A, -B, -C, and -D). HEK-293 cells were transfected with WT-RAMP2 or -3 plus WT-CLR or one of the indicated mutants. Data are shown as the means ± SEM of five experiments in (C) and five to seven experiments in (D) and are expressed as percentages of CLR/RAMP1 (C) or CLR/RAMP2 (D). $^{*}P < 0.05$ vs. corresponding CLR/RAMP.

derived from the curves are given in Table 3. When co-expressed with RAMP1, Mut-A (Hill slope = 0.65), Mut-C (Hill slope = 0.69) and Mut-D (Hill slope = 0.57) significantly reduced CGRP affinity, although Mut-B (Hill slope = 0.73) behaved much like WT-CLR (Hill slope = 0.73). These Hill slopes were not different from each other. There were no significant differences in the affinity of AM for the WT and mutant AM_1 receptors. Their Hill slopes were not different from each other, although the four Hill slopes (0.75 for CLR/RAMP2; 0.85 for Mut-A/RAMP2; 0.80 for Mut-B/RAMP2; 0.77 for Mut-C/RAMP2) differed from 1. On the other hand, Mut-A/RAMP3 significantly increased AM affin-

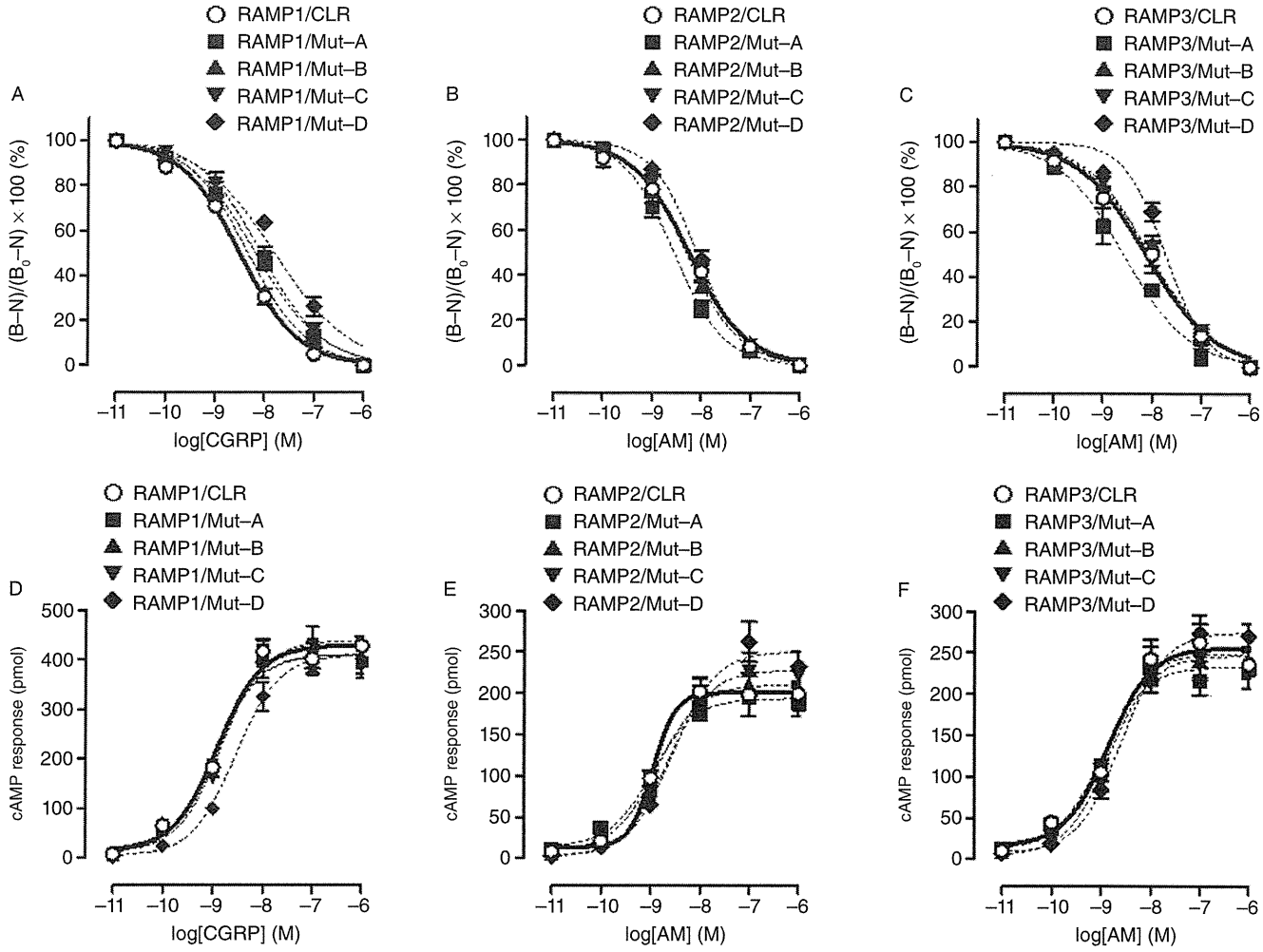

Figure 8

Effect of CLR ECL3 point mutations on agonist binding affinity and induced cAMP production. (A–C) Competitive binding of [^{125}I]-CGRP to WT or mutant CLR/RAMP1 (A) and binding of [^{125}I]-AM to WT or mutant CLR/RAMP2 (B) or CLR/RAMP3 (C). HEK-293 cells were co-transfected with WT-RAMP and WT or mutant CLR (Mut-A, -B, -C and -D). Data are shown as the means ± SEM of five experiments in (A–C). [^{125}I]-CGRP (A) or [^{125}I]-AM binding (B, C); B_o, total binding in the presence of competing unlabelled CGRP (A) or AM (B, C); N, nonspecific binding (measured in the presence of 10^{-6} M CGRP (A) or 10^{-6} M AM (B, C). pIC_{50} values are given in Table 3. (D–F) cAMP production elicited by WT or mutant CLR (Mut-A, -B, -C and -D) expressed with WT-RAMP. WT-CLR or one of the four CLR mutants was transiently transfected into HEK-293 cells along with RAMP1 (D), RAMP2 (E) or RAMP3 (F). All transfectants were then simultaneously exposed to the indicated concentrations of CGRP or AM. Data are shown as the means ± SEM of six experiments in (D) and seven experiments in (E, F). pEC_{50} values are given in Table 3.

ity, but Mut-D/RAMP3 significantly reduced AM affinity. The remaining two mutant receptors exhibited AM affinity comparable to WT AM_2 receptors. Their Hill slopes were different from each other (0.63 for CLR/RAMP3; 0.65 for Mut-A/RAMP3; 0.64 for Mut-B/RAMP3; 0.68 for Mut-C/RAMP3) because Mut-D/RAMP3 had a steeper slope of 1.04, compared to the others.

The functionality of the four CLR mutants co-expressed with RAMP1, RAMP2 or RAMP3 was evaluated by measuring CGRP- or AM-induced cAMP accumulation (Table 3, Figure 8D–F). The potency and efficacy of CGRP for the four mutant CGRP receptors were not significantly different from those for the WT CGRP receptor. Likewise, all four CLR mutants did not significantly change AM potency and efficacy in the presence of RAMP2 or RAMP3. Among all the WT and mutant receptors, only the Hill slope (1.9 for AM) of the WT AM_1 receptor was different from 1.

Discussion and conclusions

In the present study, we found that exchanging the CLR ECL3 (amino acids 395–406, including the receptor signal peptide) with the corresponding VPAC2 sequence markedly reduced AM-induced cAMP production via the AM_1 and AM_2 receptors, but CGRP-induced cAMP production via the CGRP receptor was unaffected. A very recent study showed the

Table 3

pIC_{50}, pEC_{50} and E_{max} data for WT and mutant receptors with CGRP or AM

Receptor complex	pIC_{50} ± SEM (*n*)	pEC_{50} ± SEM (*n*)	E_{max} ± SEM (pmol) (*n*)
RAMP1/WT-CLR	8.51 ± 0.04 (5)	8.90 ± 0.09 (6)	429.1 ± 11.1 (6)
RAMP1/Mut-A	8.19 ± 0.05 (5)*	8.95 ± 0.12 (6)	410.4 ± 15.0 (6)
RAMP1/Mut-B	8.34 ± 0.06 (5)	8.92 ± 0.09 (6)	409.9 ± 10.8 (6)
RAMP1/Mut-C	8.07 ± 0.06 (5)*	8.83 ± 0.11 (6)	438.3 ± 14.8 (6)
RAMP1/Mut-D	7.80 ± 0.08 (5)*	8.54 ± 0.11 (6)	409.0 ± 15.0 (6)
RAMP2/WT-CLR	8.24 ± 0.06 (5)	8.95 ± 0.04 (7)	200.8 ± 4.4(7)
RAMP2/Mut-A	8.55 ± 0.04 (5)	8.96 ± 0.15 (7)	193.7 ± 8.3 (7)
RAMP2/Mut-B	8.30 ± 0.04 (5)	8.87 ± 0.12 (7)	210.5 ± 7.4 (7)
RAMP2/Mut-C	8.23 ± 0.05 (5)	8.66 ± 0.14 (7)	228.0 ± 10.0 (7)
RAMP2/Mut-D	8.08 ± 0.03 (5)	8.55 ± 0.12 (7)	250.5 ± 9.9 (7)*
RAMP3/WT-CLR	8.13 ± 0.07 (5)	8.85 ± 0.14 (7)	256.2 ± 10.6 (7)
RAMP3/Mut-A	8.58 ± 0.07 (5)*	8.99 ± 0.15 (7)	232.6 ± 10.3 (7)
RAMP3/Mut-B	8.05 ± 0.07 (5)	8.93 ± 0.13 (7)	249.3 ± 9.8 (7)
RAMP3/Mut-C	8.07 ± 0.07 (5)	8.83 ± 0.16 (7)	246.5 ± 12.1 (7)
RAMP3/Mut-D	7.73 ± 0.05 (5)*	8.59 ± 0.11 (7)	274.6 ± 9.2 (7)

*$P < 0.05$ vs. the corresponding RAMP/WT-CLR, one-way ANOVA followed by Dunnett's multiple comparison test.
For RAMP1-based receptors: competition between CGRP and [^{125}I]-CGRP and CGRP responses.
For RAMP2- or RAMP3-based receptors: competition between AM and [^{125}I]-AM and AM responses.
AM, adrenomedullin; RAMP, receptor activity-modifying protein; WT, wild-type; CLR, calcitonin receptor-like receptor; Mut, mutant.

effect of single point mutations in the CLR ECL3 on CGRP receptor function in the presence of hRAMP1 (Barwell *et al.*, 2011). Among all the mutant receptors, only I400A/RAMP1 showed a significant reduction (~7-fold) in CGRP potency (Barwell *et al.*, 2011), although this contribution appears to be minor. In addition to I400, P396 and Y405 in CLR are also conserved in hVPAC2. All the remaining mutants, including P396A and Y405A, maintained normal CGRP responses (Barwell *et al.*, 2011). Of our four mutants, only Mut-D (D406A/Y407A/I408A) exhibited a small but significant reduction in CGRP response. Taken together, these findings suggest that the CLR ECL3 is required for appropriate activation of the two AM receptors but is less involved in CGRP receptor activation. To our knowledge, this is the first report showing the critical involvement of ECL3 in the activation of a Family B GPCR, although there is substantial evidence of the importance of ECL3 in Family A GPCR signalling (Lawson and Wheatley, 2004; Claus *et al.*, 2005; Klco *et al.*, 2006; Kleinau *et al.*, 2008; Peeters *et al.*, 2011). In these cases, reduced signalling is due largely to a loss of agonist binding. The general view is that agonist binding to GPCRs triggers a conformational change within the TM receptor core, leading to proper G-protein activation (Wess *et al.*, 2008). Our results showed that the two ECL3 chimeric receptors CH-I/RAMP2 and CH-I/RAMP3 behaved like WT receptors with respect to their specific binding and the binding affinity of [^{125}I]-AM. Therefore, it is likely that the CLR ECL3 is mainly involved in AM-induced conformational changes of the AM_1 and AM_2 receptors to induce signal activation.

Among the four mutants targeting residues within the CLR ECL3, only Mut-D showed small but significant decreases in AM potency, without affecting AM efficacy in the presence of RAMP2 or RAMP3. These results suggest that the nine amino acid residues tested, none of which are conserved in hVPAC2, are not critically involved in the activation of the two AM receptors. There is a small possibility that the remaining three residues (P396, I400 and Y405) are crucially involved in AM receptor activation because they are all conserved in hVPAC2. The hVPAC2 ECL3 shares little sequence identity with that of CLR and lacks two residues present in the CLR ECL3 (Figure 1A). Therefore, it is likely that these two differences between the ECL3 structures lead to marked reductions in AM responses via CH-I/RAMP2 or CH-I/RAMP3. Our results suggest that the entire structure of the CLR ECL3 plays a key role in AM-mediated maximal activation, which is also supported by the findings that the CLR ECL3 is highly conserved among animals despite being a non-TM region (Figure 9A).

It is well known that the receptor/G-protein complex has a higher affinity for agonists than does the free or uncoupled receptor (Zhao *et al.*, 1998). In this study, there were no significant changes in AM affinity for CH-I/RAMP2 or CH-I/RAMP3. In addition, neither of the chimeric receptors decreased their specific [^{125}I]-AM binding. These results suggest that the primary role for the ECL3 of CLR may be to control G_s activation, rather than G_s coupling, in the AM_1 and AM_2 receptors. For the AM_1 receptor, the CLR helix 8 (Figure 1B) has been suggested to be a key determinant of G_s-mediated signalling (Kuwasako *et al.*, 2010). Therefore, the entire ECL3 of CLR seems to contribute indirectly to the agonist-induced receptor conformational change for G_s activation.

Notably, CH-I/RAMP1 showed a 12-fold reduction in AM potency without affecting CGRP potency. In addition, CGRP

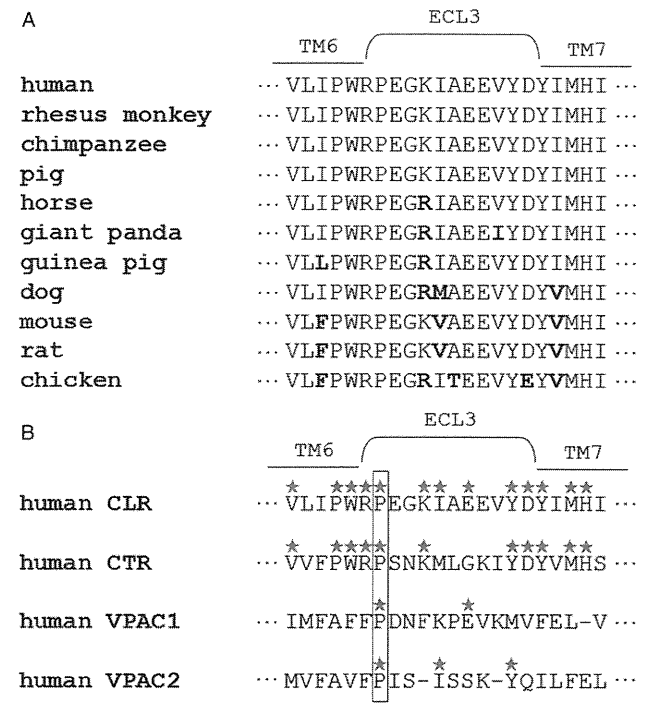

Figure 9

(A) Comparison of CLR ECL3 sequences from 11 mammals. Non-conserved amino acids are in bold. (B) Comparison of ECL3 sequences among the three human Family B GPCRs that interact with the three RAMPs: CLR, calcitonin receptor (CTR) and VPAC1 receptor. A grey asterisk indicates amino acid residues conserved in CLR. Amino acids conserved among CLR, CTR and VPAC1 are boxed.

potency for CH-I/RAMP2 and CH-I/RAMP3 was affected to a much lesser extent. These results suggest that the CLR ECL3 participates in AM signalling, but not CGRP signalling, via all three WT CLR/RAMP heterodimers. Previous studies showed that the CLR ectodomain (ECD) contains a sequence that contributes to AM binding in the presence of RAMP2; the CLR sequence was not involved in CGRP binding in the presence of RAMP1 (Koller *et al.*, 2002; 2004). The interaction between the CLR ECD and AM is supported by a 'two-domain model', which predicts that in many Family B GPCRs, agonist specificity is primarily associated with the ECD (for the C-terminus of the agonist) and with secondary recognition by a TM domain (for the N-terminus of the agonist) (Siu and Stevens, 2010). So far, there have been few reports showing that RAMPs possess critical sites for the binding of CGRP and AM (Qi and Hay, 2010; Kuwasako *et al.*, 2011b). Rather, the three RAMPs may indirectly alter the binding affinity of CGRP and AM to the ECD and TM of CLR. Taken together, it is possible that CGRP and AM may change the conformation of CLR differently within the same receptor complex. To validate our hypothesis, further work to elucidate the entire crystal structure of the three CLR/RAMP heterodimers in the presence and absence of CGRP/AM binding would be valuable.

In Family A GPCRs, ECL3 has been shown to interact with other extracellular regions (e.g. ECD, ECL2) through hydrogen bonds, disulphide bonds, etc. (Peeters *et al.*, 2011). Like Family B GPCRs, RAMPs possess a large ECD. However, none of the CLR ECL3 residues that are not conserved in VPAC2 were found to be significantly involved in interactions with RAMPs because our four CLR ECL3 mutants only slightly affected the surface delivery of RAMPs (Figure 7A and B). Among the CLR ECL3 residues, only P396 is conserved, not only in VPAC2 but also in calcitonin receptor and VPAC1 (Figure 9B). Although the three RAMPs can also interact strongly with calcitonin receptor and VPAC1 (Hay *et al.*, 2006; Sexton *et al.*, 2009), the cell-surface expression of P396A/RAMP1 was not reduced compared with the WT CGRP receptor (Barwell *et al.*, 2011). Therefore, it seems unlikely that P396A interacts with other RAMPs.

In contrast to ECL3, the replacement of CLR TM7 with the corresponding VPAC2 sequence had less of an effect on signalling via the CGRP, AM_1 or AM_2 receptor. The TM7 regions of CLR and VPAC2 are about 40% identical (Figure 1A), which raises the possibility that the nine conserved residues participate in TM7 functions shared by CLR and VPAC2. It was previously reported that, in the human VPAC1 receptor, the binding of Asp^5 of VIP to Arg^{188} in TM2 alters the interaction network between Arg^{188} and Asn^{229} in TM3 and Gln^{380} in TM7, leading to G-protein activation (Chugunov *et al.*, 2010). Notably, these three residues are fully conserved among many Family B GPCRs, suggesting that there may be a common mechanism underlying Family B GPCR activation. Consistent with this idea, Glu^{380} in VPAC1 is strictly conserved in CLR and VPAC2. Additional experiments are needed to confirm whether this activation mechanism also applies to both CLR and VPAC2.

In summary, the human CLR ECL3 is crucial for AM-induced cAMP responses via the three CLR/RAMP heterodimers but is less involved in their CGRP responses. This CLR region probably participates in AM-induced conformational changes of these heterodimers and thereby induces their activation. This study provides a clue to the molecular basis of the activation of RAMP-based Family B GPCRs.

Acknowledgements

This study was supported in part by Grants-in-Aid for Scientific Research from the Ministry of Education, Culture, Sports Science and Technology, Japan and by research grants from the Takeda Science Foundation, the Mochida Memorial Foundation for Medical and Pharmaceutical Research and the Suzuken Memorial Foundation.

Conflict of interest

The authors state that they have no conflict of interest.

References

Bailey RJ, Hay DL (2007). Agonist-dependent consequences of proline to alanine substitution in the transmembrane helices of the calcitonin receptor. Br J Pharmacol 151: 678–687.